Optimization of iron analyses using ESI-MS: Detection of iron oxide in pharmaceuticals

Dendi Susanto

A Thesis

in

The Department

of

Chemistry and Biochemistry

Presented in Partial Fulfillment of the Requirements
for the degree of Master of Science (Chemistry) at
Concordia University
Montreal, Quebec, Canada

April 2009

CONCORDIA UNIVERSITY

Canada

ABSTRACT

Optimization of iron analyses using ESI-MS: Detection of iron oxide in pharmaceuticals

Dendi Susanto

Detection of iron oxide in pharmaceutical formulations using electrospray ionization mass spectrometry (ESI-MS) following iron complexation with 1,10-phenanthroline (Phen), 1-(2-pyridylazo)-2-naphthol (PAN), and 4-(2-pyridylazo)resorcinol (PAR) was evaluated. Complexation of Fe^{III} with PAR was found to produce a distinctive and sensitive mass spectral signal when compared to the other ligands. In selected ion monitoring (SIM) scan mode, the signal at m/z 484 arising from the iron-PAR complex gave a limit of detection of 2 μM for total iron using a triple-quadrupole mass spectrometer. The range of the calibration curve was determined to be 2 – 43 μM total iron. Trace iron interferences from the labware and instrumentation were minimized considerably by selection of an optimized cleaning protocol and instrument replumbing using PEEK® tubing. Figures of merit for total iron analysis (specificity, linearity, precision and accuracy, robustness, and stability) were within the acceptance criteria of the US FDA validation guidelines for the pharmaceutical industry. Recovery of 93% of the added iron indicated a satisfactory extraction procedure for tablets containing iron oxide pigment. There was no statistical difference between the results obtained by ESI-MS and a conventional method such as inductively coupled plasma-optical emission spectroscopy (ICP-OES). The proposed ESI-MS method was found to be specific, sensitive, and relatively inexpensive since it can be performed on a mass spectrometer

equipped with an ESI source, which is standard instrumentation in the pharmaceutical industry. Thus, the method validated here provides an alternative to laboratories that do not have specialized and dedicated instrumentation for elemental analysis.

Dedication

This thesis is dedicated to my little daughter, Angelika-Lili, who is 4½ years at the time of writing. I certainly hope, when she grows up she can read this page and understand what her daddy went through. Hopefully, not only will she understand what I achieved but she will be more motivated and determined to excel.

List of Figures

List of Tables

List of Acronyms

AAS	Atomic Absorption Spectrosphotometry
API	Active Pharmaceutical Ingredient
ESI	Electrospray Ionization
HCl	Hydrochloric acid
HPLC	High Performance Liquid Chromatography
ICP-OES	Inductively Coupled Plasma - Optical Emission Spectroscopy
ID	Inner Diameter
LOD	Limit of Detection
LOQ	Limit of Quantitation
MALDI-TOF	Matrix Assisted Laser Desorption Ionization Time of Flight
MS	Mass Spectrometry
OD	Outer Diameter
PAN	1-(2-Pyridylazo)-2-Naphthol
PAR	4-(2-Pyridylazo)Resorcinol
Phen	1,10-Phenanthroline
RRHT	Rapid Resolution High Throughput
SIM	Selected Ion Monitoring
S/N	Signal-to-Noise ratio
TFA	Trifluoroacetic acid
TIC	Total Ion Current
US FDA	United States Food and Drug Administration
UV-Vis	UltraViolet-Visible

Chapter 1   General Introduction

The following thesis describes the determination of total iron in pharmaceutical products containing iron oxide pigment. The suitability of ligands for quantitative analysis was investigated. Method validation figures of merit for quantitative analysis are discussed in Chapter 2. The behaviour of the metal ion complexes noted during method development is described in Chapter 3. Finally, concluding remarks and suggestions for future work are presented in Chapter 4.

The scope of this thesis is to determine the total iron present in pharmaceutical products using a mass spectrometer equipped with an electrospray (ESI) source. Since this method will be adopted for pharmaceutical use, the method validation figures of merit are based on the regulatory guidelines, especially those of the United States Food and Drug Administration (US FDA). Investigations of other techniques will not be discussed in this thesis.

Colors from synthetic pigments are used in pharmaceutical finished products for identification, appearance, as well as product stability. Only a handful of pigments are approved by the regulatory agencies worldwide, including the US FDA. The approved pigments are indigo carmine, brilliant blue, sunset yellow, titanium dioxide, and iron oxide [1]. Synthetic pigment containing iron oxide, Fe_2O_3, which represents one of the excipients in pharmaceutical formulations, not only gives an appealing color to the final drug product, but it also protects the active pharmaceutical ingredients (APIs) from degradation upon exposure to light [2]. Iron oxide is added to drug products as a blend in the granulation or as a film coating to a core tablet [3].

The FDA requires that synthetic iron oxide pigment is not more than 3% w/w of the total tablet weight and the pigment must not contain more than 55% Fe_2O_3. Currently, specification of the iron oxide content in a tablet is not part of the release requirement for pharmaceuticals manufacturers. However, it is part of the batch record, which clearly identifies all formulation ingredients. The pigment is accounted for in a tablet formulation by the percent weight composition of overall tablet weight. The current release requirements of the drug product consist only of an identification test to confirm the existence of the pigment in the tablet [4]. This will change in a few years as the United States Pharmacopeia, the pharmaceutical standard-setting organization in the US, proposes new standards for pharmaceutical manufacturers to report metal content in their products, as recently described in Chemical and Engineering News [5].

Common methods for elemental analysis such as colorimetry involve complexation of metal ions with appropriate ligands to form complexes that exhibit strong UV-Vis absorbance. However, this procedure can suffer from spectral interference when more than one metal species is present, and therefore mathematical derivatisation techniques are used to overcome this problem [6, 7].

HPLC-based methods also require metal ions to be complexed if reversed-phase chromatography is to be used [8]. This approach requires analytical method development to separate the metal ions of interest. In addition, HPLC can offer metal-ion separation without the need for complexation. This approach, ion chromatography, requires a special HPLC instrument made of metal-free components to achieve the separation goals without interference [9].

Atomic absorption spectrophotometric (AAS) methods, with either flame or

graphite furnace atomization, offer direct analysis of metal content. One metal is generally analyzed at the time, so throughput limitation results in lengthy sample processing that is time consuming and labour intensive [10, 11].

Inductively coupled plasma (ICP) analysis coupled with mass spectrometry (MS) or optical emission spectroscopy (OES) is the ideal choice for elemental analysis. These methods are capable of running multi-element analyses simultaneously, thereby giving a high throughput advantage over other techniques [12, 13]. The disadvantages of ICP methods are the high overhead cost of operating the instrumentation as well as the need for skilled operators, especially in the case of ICP-MS. These drawbacks deter many laboratories from purchasing instrumentation dedicated to elemental analyses.

Matrix assisted laser desorption ionization – time of flight mass spectrometry (MALDI-TOF MS) methods make use of ligands that complex the metal ion of interest as a matrix in the ionization process. The sample exists as a solid and the laser beam creates ionization. The resulting mass spectrum confirms formation of the complex ion of the desired metal ions with ligands [14]. For example, Matsumoto et al. [14] have shown that iron oxides can be detected using MALDI-TOF MS when 1-(2-pyridylazo)-2-naphthol (PAN), 4-(2-pyridylazo) resorcinol (PAR) or 1,10-phenanthroline (Phen) are employed as MALDI matrices to complex the iron. MALDI-TOF MS is good for qualitative and screening purposes. However, it lacks the quantitative power to determine the amounts of the metal ions in the samples [15].

Electrospray ionization mass spectrometry (ESI-MS), on the other hand, is used in many laboratories for multiple types of analyses, including metal ion analysis. Using this approach, the metals also need to be complexed with appropriate ligands due to

limitations of ESI-MS detection. Nonetheless, ESI-MS provides an alternative for the qualitative and quantitative analyses of metal-ligand complexes [16, 17].

ESI-MS was developed as a useful and versatile tool following the work of Fenn [18] in the early 1980s. In this process, a solution is passed through a small capillary tube which produces charged spray droplets on applying a high electric potential. As the solvent is evaporated, the charge density becomes higher until coulombic repulsion takes place breaking the bigger droplets into smaller ones. This process continues until the analyte ions are essentially desolvated and accelerated toward the mass analyzer. The advantage of ESI is the ability to elucidate the structure of molecules and their properties, hence its use in many applications.

Since quantitation by MALDI-TOF MS is limited as previously mentioned, ESI-MS analysis of iron was explored here. This thesis will demonstrate the capability of ESI-MS for total iron analysis from pharmaceutical tablets containing synthetic iron oxide pigments. Method optimization and validation, as well as metal ion behaviour are outlined in the following two chapters.

To confirm the validity of the method developed, a comparative study was performed by ICP-OES. While ESI-MS is unlikely to replace elemental analysis by ICP-OES, ICP-MS or AAS, it can provide an alternative when dedicated instruments are not available. The ESI-MS method developed here not only offers advantages in selectivity over common techniques such as colorimetry, it also offers simplicity. Extensive analyte separation by chromatographic methods is not required because of the mass resolution of the mass spectrometer.

Chapter 2   Development and validation of a quantitative method for iron in pharmaceutical products

2.1   Introduction

In this chapter, ESI-MS method validation figures of merit for quantitative analysis of total iron in pharmaceutical tablets are discussed. Using ligands from the MALDI-TOF MS work of Matsumoto et al. [14], evaluation of ESI-MS for total iron analysis was carried out. Figures of merit were established using the best ligand. Tablets containing iron oxide pigment were measured for total iron using the validated method. To ensure the validity of the method, the results were compared with those obtained using ICP-OES.

2.2   Experimental

2.2.1   Materials

The following chemicals were obtained from Sigma-Aldrich (St. Louis, MO, USA): 1,10-phenanthroline monohydrate, 1-(2-pyridylazo)-2-naphthol (PAN, anhydrous free base, indicator grade 98%), 4-(2-pyridylazo) resorcinol (PAR, anhydrous free base, indicator grade 98%), hydroxylamine HCl (ACS Reagent, 99%), NH_4OH (98% certified) and L-ascorbic acid (99% certified). Formic acid (mass spectrometry grade, puriss >98%) was obtained from the Fluka, division of Sigma-Aldrich. Thermo Fisher Scientific (NY, USA) was the supplier of ammonium formate (HPLC grade, 99%), and sodium hydroxide (10 N, certified reagent), methanol and acetonitrile (HPLC grade). Concentrated HCl solution (plasma pure grade) was from SCP Science (Baie d'Urfé,

Québec, Canada). The iron standard for atomic absorption spectroscopy (1000 ppm) was obtained from Ricca Chemical Co (Arlington, TX, USA). Pharmaceutical film-coated and compressed tablets containing iron oxide pigments were available from Merck Frosst Canada Ltd, a division of Merck & Co. (NJ, USA). Synthetic pigment containing iron oxide for qualitative evaluation was obtained from Elementis Pigment (Fairview Hill, IL, USA). Ultrapure double-deionized water was obtained from a Milli-Q water purification system (Bedford, MA, USA). PEEK® tubing was obtained from VICI Valco Instruments (Houston, TX, USA).

2.2.2 Instrumentation

ESI-MS analysis was carried out initially using a LCQ Deca® ion trap mass spectrometer fitted with an electrospray ionization source (ThermoQuest Finnigan, San Jose, CA, USA). To enhance sensitivity of detection, a triple quadrupole mass spectrometer (TSQ7000) fitted with an electrospray ionization source (ThermoQuest Finnigan, San Jose, CA, USA) was additionally used. Data were acquired and processed with Xcalibur 2.0 software. The mass spectrometer was mass calibrated using standard calibration solutions, Ultramark 1621, MRFA (peptide Met-Arg-Phe-Ala) (Alfa Aesar, Ward Hill, MA, USA) and caffeine (Sigma-Aldrich, St. Louis, MO, USA). The instruments were operated in positive-ion mode and instrumental parameters were optimized using the Autotune® feature of Xcalibur for solutions containing dissolved iron and ligand at the expected mass-to-charge ratio of the complex molecules. Samples (50 µL) in 50% acetonitrile/ 0.1% formic acid (v/v) were analyzed by direct-flow injection from an 1100 HPLC system (Agilent Technologies, Palo Alto, CA, USA) at a flow rate

of 1 mL/min and split at 120 µL/min to the ESI source. Table 2.1 summarizes the optimal

source parameters for free ligand analysis using the ion trap mass spectrometer, and

Table 2.2 summarizes the optimal conditions for the quantitation of total PAR-bound iron

using the triple quadrupole mass spectrometer. Mass spectral scans were recorded

between m/z 100 and 1000 at a scan time of 1 min.

Table 2.1: ESI source parameters for free ligand detection using the LCQ DECA ion trap mass spectrometer[a]

Parameters	Phen (m/z 181)	PAN (m/z 250)	PAR (m/z 216)
ESI source voltage (kV)	+5	+5	+5
Heated capillary voltage (V)	+17	+3	+4
Tube lens offset (V)	+5	-25	-20
Heated Capillary Temp (°C)	350	350	350
Nitrogen sheath gas flow rate [b]	63	63	63
Nitrogen aux. gas flow rate [b]	27	27	27

[a] Operated in positive-ion mode with 8 µM PAN, 10 µM PAR dissolved in 50% aq methanol/0.1% formic acid (pH 2.5) and 25 µM of phen in 50% aq methanol/20 mM ammonium formate pH 3.5. Sample solutions were infused using a 250-µL Hamilton syringe at a flow rate of 10 µL/min. [b] Arbitrary units

Table 2.2: ESI source parameters for total iron quantitation complexed by PAR using the TSQ7000 triple quadrupole mass spectrometer[a]

Parameters	m/z 484
ESI source voltage (kV)	+4.5
Capillary voltage (V)	+33.7
Capillary offset voltage (V)	+68.0
Lens 1-1 voltage (V)	-3.0
Heated Capillary Temp (°C)	350
Nitrogen sheath gas flow rate [b]	80
Nitrogen aux. gas flow rate [b]	20

[a] Operated in positive-ion mode with 50 μL solution containing 43 μM Fe^{III} standard and 233 μM PAR in 50% aq acetonitrile. The mobile phase was 50% aq acetonitrile/0.1% formic acid (pH 2.5) delivered from an HPLC with a flow rate of 120 μL/min. [b] Arbitrary units

Absorbance readings in the colorimetric analysis of iron were measured on a Model 8453 diode-array spectrophotometer (Agilent Technologies, Palo Alto, CA, USA), and solution pH values were monitored using a Thermo Orion 920A+ pH meter with a glass-filled electrode (Thermo Electron, San Jose, CA, USA).

ICP-OES analyses were carried out using an iCap 6500 ICP-OES (Thermo Electron, San Jose, CA, USA) with argon gas as a nebulizer. The sample flush time was set at 30 s and the plasma was generated using a RF power of 1150 W. The nebulizer gas flow was set at 0.7 L/min and the auxiliary gas flow at 0.5 L/min. The 259.9-nm emission line of iron, which corresponds to its strongest emission, was used for its detection and quantitation. This emission line is selected from the internal database in the iCap when iron is analyzed. Triplicate measurements at 259.9 nm were recorded for each sample and average values are reported (Section 2.4.5).

2.2.3 Labware and cleaning protocols

To minimize interference from trace iron found in materials, specialized labware was used throughout the experiments. Polycarbonate-based volumetric flasks from Nalgene (Thermo Fisher Scientific, NY, USA) were employed in sample and calibrant preparation. The flasks were subjected to the standard company (Merck Frosst) pre-wash cleaning procedure for labware prior to use. The pre-wash consisted of the following steps:

- Labware was soaked overnight with absolute ethanol, and rinsed with tap water.

- Labware was loaded into the washer (Labconco, Missouri, USA) with the following cycles:

  o Wash cycle with soap containing tetrasodium EDTA (Glass Klenz, Steris, St. Louis, Mo, USA) at room temperature (30 min).

  o Rinse cycle with double deionized Milli-Q water at room temperature (30 min).

  o Wash cycle with soap containing 25% w/w citric acid (Calgon Vestal Labs, Bramalea, Ont, Canada) at room temperature (30 min).

  o Rinse cycle with double deionized Milli-Q water at room temperature (30min)

  o Labware was then loaded into oven (70°C for 1 h) or until dry.

After the company wash, volumetric flasks were additionally rinsed 3x with 10% HCl (plasma pure grade), and rinsed 3x with Milli-Q water.

2.2.4 Calibration curve preparation

Calibration and quality-control samples were prepared by diluting the appropriate

volume of intermediate standard solutions into 50-mL Nalgene volumetric flasks as summarized in Table 2.3. Intermediate solutions were prepared from the standard Fe stock solution (Ricca Chemical Co, TX, USA) by diluting the volume indicated in Table 2.3 into a 100-mL volumetric flask and adjusting to the mark with Milli-Q water. With a graduated cylinder, 25 mL of 465 μM PAR, prepared freshly in acetonitrile, was added to each flask, and adjusted to the mark with Milli-Q water. A matrix blank was prepared in the same manner as the calibration samples by replacing the intermediate standard solution with Milli-Q water. Uniform mixing was ensured by inverting the volumetric flask 3 times and the solutions were left standing overnight at ambient laboratory conditions before assay.

Table 2.3: Preparation of standards (Std) and quality control (Qc) samples for total iron analysis[a]

	Intermediate A (20 ppm Fe)	2 mL of stock (1000 ppm Fe) in 100 mL of Milli-Q H_2O			
	Intermediate B (1 ppm Fe)	5 mL of Intermediate A in 100 mL of Milli-Q H_2O			
	Concentration μM (ppm Fe)	Vol of Intermediate A (mL)	Vol of Intermediate B (mL)	Vol of 465 μM PAR (mL)	Total Vol (mL)
Std A	2.14 (0.12)	-	6	25	50
Std B	5.71 (0.32)	-	16	25	50
Std C	14.29 (0.80)	2	-	25	50
Std D	28.57 (1.60)	4	-	25	50
Std E	42.86 (2.40)	6	-	25	50
Qc A	7.14 (0.40)	-	20	25	50
Qc B	35.71 (2.00)	5	-	25	50

[a] Stock solution, 1000 ppm Fe in 3% aq HCl (Ricca Chemical Co, TX, USA)

2.2.5 Tablet extraction procedure

Ten intact tablets per flask, each tablet weighing approximately 100 mg, were added into 50-mL Nalgene volumetric flask. Into each flask, 2mL of water was added to help disintegrate the tablets, and after complete disintegration, 20 mL of concentrated HCl (Plasma pure grade) was added. The flasks were placed in an ultrasonic bath for 30 min and shaken vigorously at 15-min interval for approximately 1 min to ensure complete extraction. At end of sonication, Milli-Q water was added to below the mark, and the solutions were left to cool at room temperature before adjusting to the mark with Milli-Q water. A 13-mL portion was transferred into a 15-mL Eppendorf tube for centrifugation at 3500 rpm for 15 min. With a glass volumetric pipette, 10 mL of the supernatant was transferred into a clean 50-mL volumetric flask and adjusted to the mark with Milli-Q water.

With a clean volumetric pipette, 10 mL of the diluted solution was transferred into a clean beaker, and the pH was adjusted to ~ 1.8 with the dropwise addition of 15 M aqueous NH_4OH and then the dropwise addition of 1 M NH_4OH to prevent overshooting the desired pH of ~ 2.3. This solution was transferred quantitatively to a clean 50-mL volumetric flask, and 25 mL of 465 μM PAR in acetonitrile was added from a graduated cylinder. The beaker was rinsed a few times with Milli-Q water, the rinsings were added to the volumetric flask, and the solution was adjusted to the mark with Milli-Q water. The sample was left standing overnight at ambient laboratory conditions before assay.

2.3 Qualitative evaluation of ligands for ESI-MS analysis of iron

To enable the detection of the iron in the samples, ligands were examined based on the study by Matsumoto et al. [14]. The absorption spectra of the free ligands evaluated in this thesis are shown in Figure 2.1, and their structures and properties are summarized in Table 2.4.

Solubilization of iron oxide requires a strong acid such as concentrated HCl [19]. In this evaluation, pigment containing iron oxide was solubilized in 500 ppm aq HCl. A working pigment solution was prepared by diluting 2 mL of the stock pigment solution into a 100-mL volumetric flask, and adjusting to the mark with Milli-Q water.
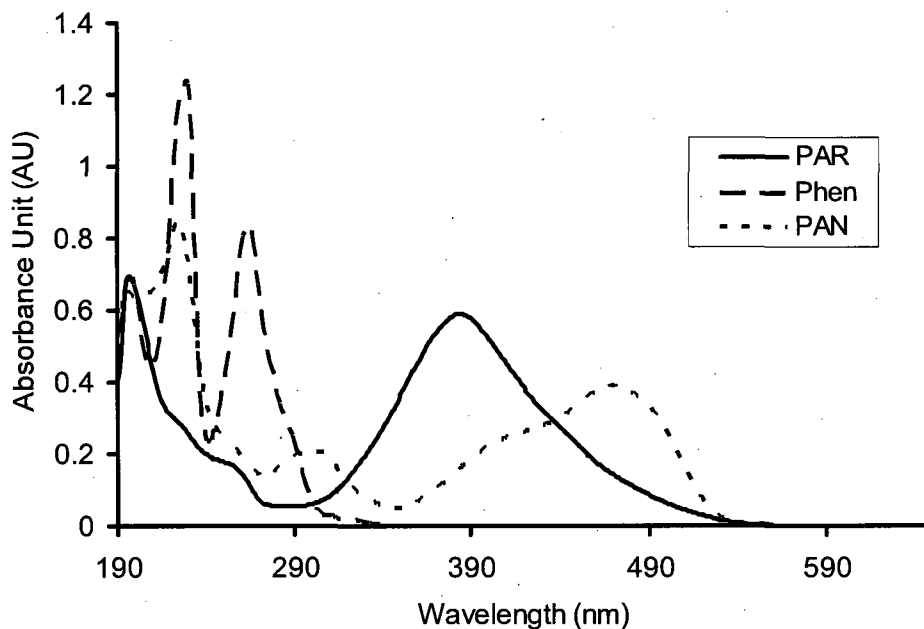
Figure 2.1: UV-Vis absorption spectra of free ligands. Spectra were recorded in a 1-cm cuvette. Ligands were dissolved in methanol to give 50 µM Phen, 16 µM PAN, and 19 µM PAR at ambient temperature.

Table 2.4: Structures of free ligands and their properties relevant to iron chelation [a, b]

1,10-phenanthroline (Phen) [20, 21]	1-(2-pyridylazo)-2-naphthol (PAN) [21, 22]	4-(2-pyridylazo)resorcinol (PAR) [21, 23]
M_r 180.21 u	M_r 249.27 u	M_r 215.21 u
Bidentate ligand	Bi- or tridentate ligand	Bi- or tridentate ligand
pK 4.96	pK_1 2.3, pK_2 12.3	pK_1 2.7, pK_2 5.5 (para-OH),
$Fe^{II}L_3$ complex (M_r 298 u)	$Fe^{III}L_2$ complex (M_r 552 u)	pK_3 12.3
λ_{max} 510 nm	λ_{max} 765 nm	$Fe^{III}L_2$ complex (M_r 484 u)
ε_{510} 1.12×10^4 $M^{-1}cm^{-1}$	ε_{765} 2.7×10^4 $M^{-1}cm^{-1}$	λ_{max} 500 nm
		ε_{500} 5.60×10^4 $M^{-1}cm^{-1}$

[a] Coordinating atoms are shown in red. [b] Fully protonated forms of the ligands are shown. Solvents were 0.05 M aq sulphuric acid (pH <1) for Phen [20], dichloromethane for PAN [22], 0.01 N aq HCl (pH adjusted to 8.8-10.3) for PAR [23], other data were taken from [21].

2.3.1   1,10-Phenanthroline (Phen)

Fe^{3+} is reduced to Fe^{2+} by NH_2OH according to equation 2.1. Three mole equivalents of Phen complex with each mole equivalent of Fe^{2+} to form $[Fe^{II}(Phen)_3]^{2+}$ (eq. 2.2). The complex is stable between pH 3 and 9 [24].

$$Fe^{3+} + NH_2OH + OH^- \rightleftharpoons Fe^{2+} + \tfrac{1}{2} N_2 + 2\, H_2O \qquad\qquad 2.1$$

$$Fe^{2+} + 3\ Phen \rightleftharpoons [Fe^{II}(Phen)_3]^{2+} \qquad\qquad 2.2$$
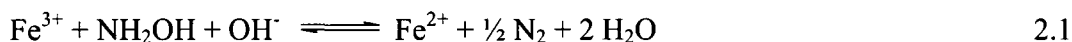
A 6-mL aliquot of 10 ppm pigment in ~ 0.24 N HCl and 1 mL of 1.44 mM NH_2OH in Milli-Q water, and 20 mL of 125 µM Phen in 100% methanol were diluted to 50 mL with 20 mM ammonium formate (pH 3.5) to yield a solution that contains ~ 7.5

μM Fe^{III} and 50 μM Phen. ESI mass spectra were recorded following direct flow injection of the samples from the HPLC to the ion trap MS. The ESI mass spectrum exhibits the MH^+ ion of free Phen at m/z 181 as the base peak (Figure 2.2). The medium intensity peak at m/z 208 corresponds to the doubly charged ion of the $[Fe^{II}(Phen)_2]^{2+}$ complex as indicated by the half integer spacing between the isotopic peaks (Figure 2.2A, inset). Evidence for the formation of the $[ClFe^{II}(Phen)_2]^+$ complex ion at m/z 451 is obtained from the isotopic pattern (3:1, M:M+2) of the chloride ion apparent in the zoom scan shown in Figure 2.2B.

Although the $[Fe^{II}(Phen)_3]^{2+}$ complex was not observed at m/z 298 in the mass spectrum, the UV-Vis absorption spectrum (Figure 2.3) of the 7.5 μM Fe^{III} / 50 μM Phen solution described above exhibits a visible maximum at 510 nm with an absorbance of 0.1 AU confirming the complexation of all the iron as $[Fe^{II}(Phen)_3]^{2+}$. Formation of $[Fe^{II}(Phen)_3]^{2+}$ is widely used in the spectrophotometric determination of iron [20, 24, 25]. The complex is characterized by its red-orange color and distinctive visible absorption maximum at 510 nm as shown in Figure 2.3.The number of ion counts in the ESI mass spectrum was on the order of 10^8 for the base peak (MH^+ ion of Phen) indicating efficient ionization of free Phen under the conditions used (50% aq methanol/20 mM ammonium formate pH 3.5).

Ion count=8.9E8
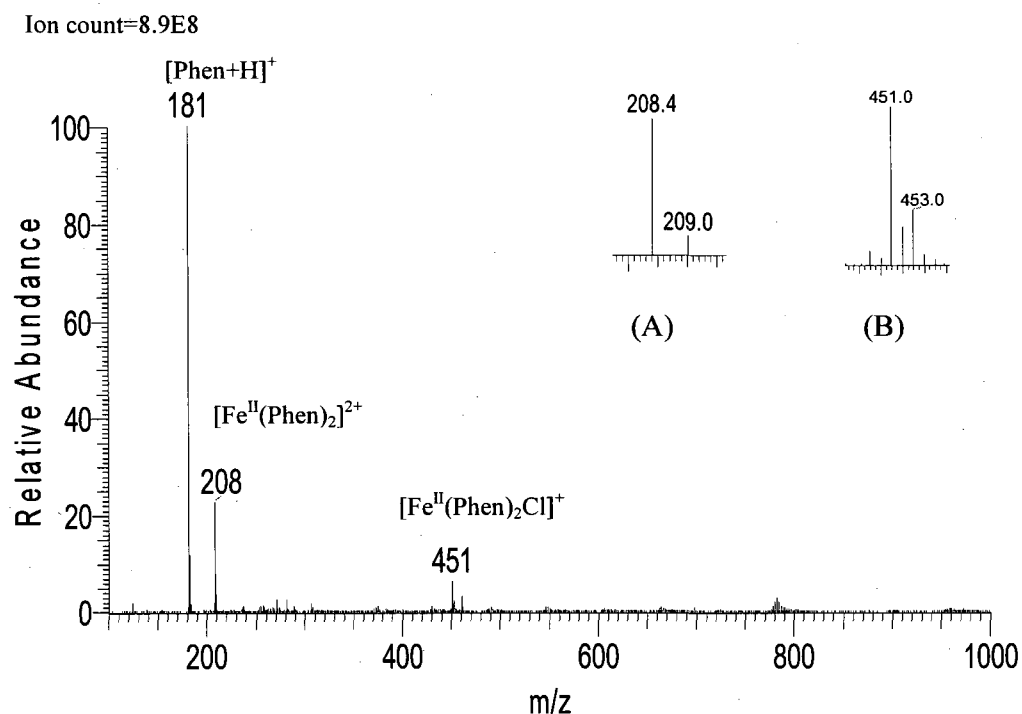
Figure 2.2: ESI mass spectrum of solution containing 7.5 μM pigment-derived iron and 50 μM Phen. The iron solution was prepared by mixing 6 mL of 10 ppm pigment in ~ 0.24 N aq HCl, 1 mL of 1.44 mM NH_2OH in Milli-Q water, 20 mL of 125 μM Phen in 100% methanol, and diluting to 50 mL with 20 mM ammonium formate pH 3.5. A 50-μL sample aliquot was directly injected with the mobile phase (50% aq methanol/20 mM ammonium formate pH 3.5) at a flow rate of 1 mL/min and split at 120 μL/min to the ion source. The heated capillary temperature was set at 350°C. Insets (A) and (B) are expanded views at the m/z values of the ions of interest. The mass spectrum was obtained with a 1-min scan time, and each scan was set at 50 ms.
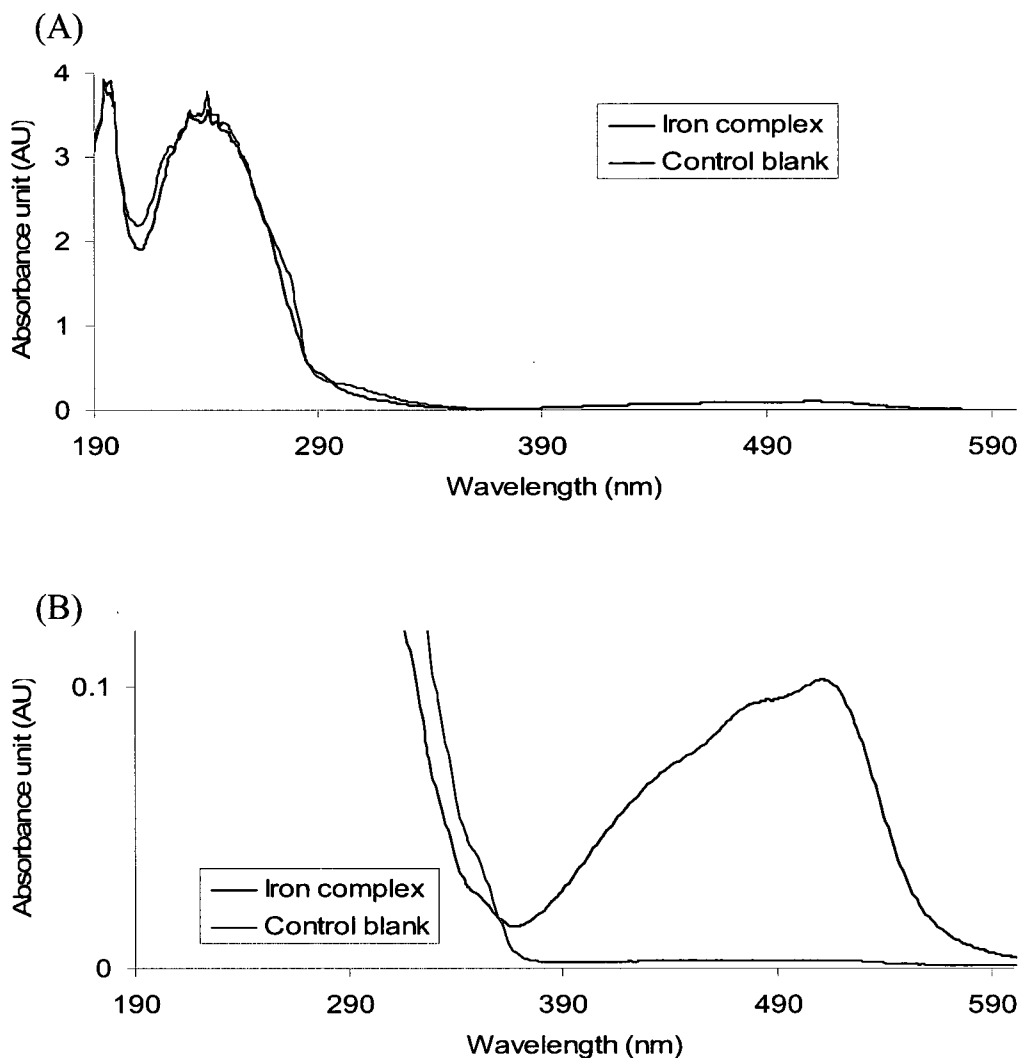
Figure 2.3: UV-Vis absorption spectrum of [Fe^{II}(Phen)$_3$]$^{2+}$. (A) 1x spectrum. (B) 40x spectrum. Absorbance readings were taken in a 1-cm cuvette. The iron solution was prepared by mixing 6 mL of 10 ppm pigment in ~ 0.24 N aq HCl, 1 mL of 1.44 mM NH$_2$OH in Milli-Q water, 20 mL of 125 μM Phen in 100% methanol, and diluting to 50 mL with 20 mM ammonium formate pH 3.5.

Since the expected tris complex, $[Fe^{II}(Phen)_3]^{2+}$, was not detected as a doubly charged ion at m/z 298, it was suspected that this ion picked up two chloride ions to form a neutral species that would not be detected by ESI-MS. To prevent the formation of the putative neutral complex $Cl_2[Fe^{II}(Phen)_3]$, attempts were made to dissolve iron oxide pigment in alternate acids such as concentrated HNO_3, H_2SO_4 or H_3PO_4. These were not successful due to the limited solubility of the oxide. Changing the mobile phase from ammonium formate (pH 3.5) to formic acid (pH 2.5) also did not lead to detection of the tris complex by ESI-MS under the conditions used in this experiment. Keki et al. have established a simple method for estimating activation energies for a collision-induced dissociation of $[Fe^{II}(Phen)_3]^{2+}$ and related complexes by ESI-MS. The complexes were prepared in water [26], which would have been impossible here due to insolubility of iron oxide in water. To release iron from the iron oxide, concentrated HCl acid is required.

To further investigate the failure to detect the $[Fe^{II}(Phen)_3]^{2+}$ complex by ESI-MS, $FeSO_4$, a salt that is highly soluble in water, was used to prepare an Fe^{2+} solution. The iron was at the same concentration used previously except that hydroxylamine reduction (eq. 2.1) was not required in this case. A $[Fe^{II}(Phen)_3]^{2+}$ solution was prepared in water and approximately 10 µL of 1 M HCl was added to one aliquot. A peak at m/z 298 was expected in the mass spectrum of the solution without HCl but not in the solution with HCl. Figure 2.4 reveals that the mass spectrum did not exhibit a peak at m/z 298 in the absence of added HCl. Another reason for the failure to detect the tris complex may be thermal degradation of the complex in the heated capillary. On lowering the capillary temperature from 350°C to 150°C, the peak at m/z 298 became the base peak (Figure 2.5C). With the heated capillary temperature set at 150°C, the solution containing HCl

was injected and the base peak was also at m/z 298 (Figure 2.5D). This suggests that the $[Fe^{II}(Phen)_3]^{2+}$ complex is thermally labile in an ESI source equipped with a heated capillary above 150°C. But with heated capillary temperature set at 150°C, the mass spectrum of the acidified solution is noisy and shows many cluster ions due to the ineffecient desolvation (Figure 2.5D). Thus, other iron ligands were examined for their ability to form stable complexes in the ESI source.
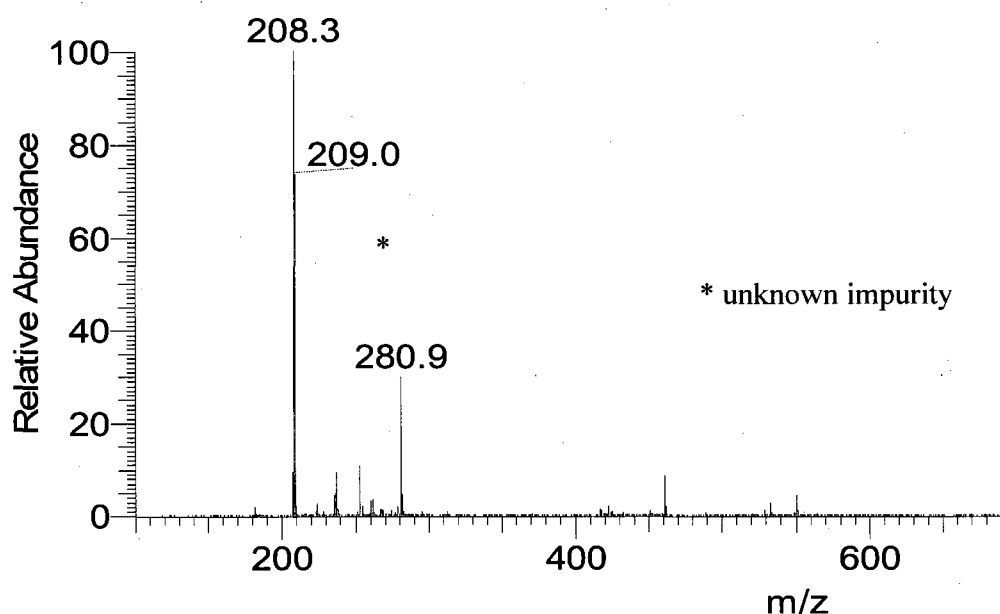
Figure 2.4: ESI mass spectrum of an aqueous solution of 7 µM FeSO₄ with 50 µM Phen in 40% aq methanol/20mM ammonium formate pH 3.5. The iron solution was prepared by mixing 6 mL of 60 µM FeSO₄ in Milli-Q water with 20 mL of 125 µM Phen in 100% methanol, and diluting to 50 mL with 20 mM ammonium formate pH 3.5. A 50-µL sample aliquot was directly injected with the mobile phase (50% aq methanol/20 mM ammonium formate pH 3.5) at a flow rate of 1 mL/min and split at 120 µL/min to ion source. The heated capillary temperature was set at 350°C. The mass spectrum was obtained with a 1-min scan time, and each scan was set at 50 ms.
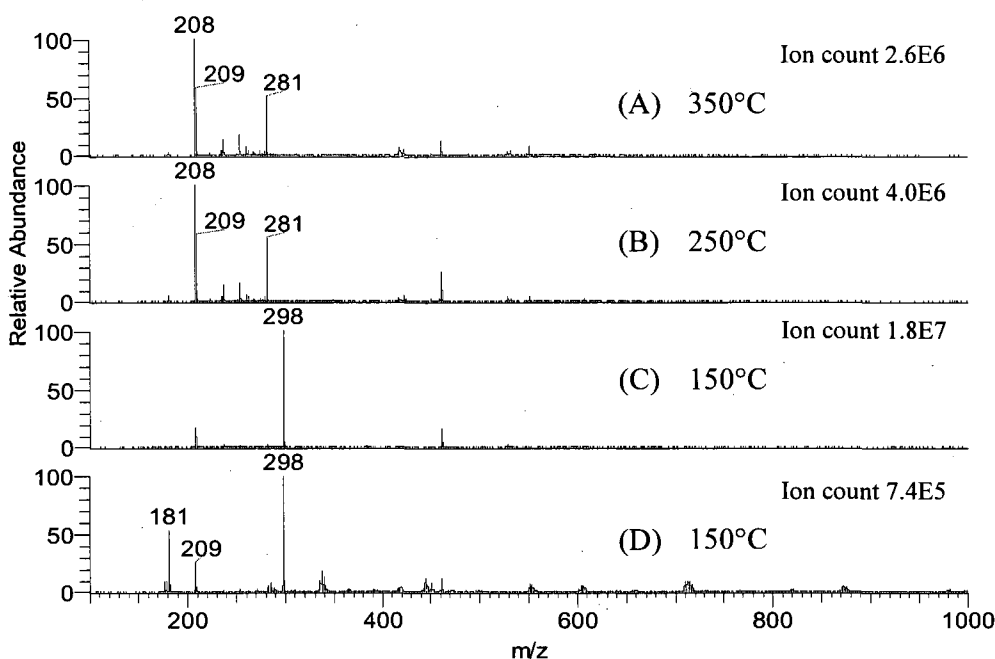
Figure 2.5: ESI mass spectra of aqueous solutions of 7 μM FeSO$_4$ and 50 μM Phen in 40% aq methanol/20mM ammonium formate pH 3.5 (A-C) without HCl (D) with 10 mM HCl. The iron solution was prepared by mixing 6 mL of 60 μM FeSO$_4$ in Milli-Q water with 20 mL of 125 μM Phen in 100% methanol, and diluting to 50 mL with 20 mM ammonium formate pH 3.5. A 50-μL sample aliquot was directly injected with the mobile phase (50% aq methanol/20 mM ammonium formate pH 3.5) at a flow rate of 1 mL/min and split at 120 μL/min to ion source. The heated capillary temperature was set at 350°C. The mass spectrum was obtained with a 1-min scan time, and each scan was set at 50 ms.

2.3.2   1-(2-pyridylazo)-2-naphthol (PAN)

An alternate ligand to Phen was evaluated because of difficulties in detecting the [Fe^{II}(Phen)$_3$]$^{2+}$ complex by ESI-MS. Reactions using PAN were carried out at low pH (< 2.5) and high pH (> 10) close to the pK$_a$ values of PAN's coordinating groups (Table 2.4). Two 50-mL solutions containing 7.5 μM Fe^{III} and 16 μM PAN (final concentrations) were prepared from 6 mL of 10 ppm pigment solution in ~ 0.24 N aq HCl. After adjusting the pH to 11 and 2.4 with dropwise addition of 1 N NaOH, 20 mL of 40 μM

PAN (final concentration) in 100% methanol was added, and the volume was adjusted to 50 mL with Milli-Q water. The ESI mass spectra are shown in Figure 2.6. The MH^+ ion of free PAN at m/z 250 is the base peak in all spectra except that recorded at pH 2.4 in the presence of pigment-derived iron (Figure 2.6D). In this spectrum, a single high intensity peak at m/z 552 is assigned to the $[Fe^{III}(PAN)_2]^+$ complex. However, at both pHs, there is interference at m/z 552 (Figure 2.6A and 2.6C), suggesting the presence of iron in the reagents. In contrast, at pH 11 there is little difference between the spectra of the PAN solutions with and without iron pigment (Figure 2.6B and 2.6A). The use of this ligand was abandoned, and another iron ligand was explored.

2.3.3   4-(2-pyridylazo)resorcinol (PAR)

A third ligand was examined to determine if the iron content can be reliably quantitated by ESI-MS. Evaluation with PAR was also carried out at low pH (< 2.5) and high pH (> 10) close to the pK_a values of PAR's coordinating groups (Table 2.4). Two 50-mL solutions containing 7.5 µM Fe^{III} and 19 µM PAR (final concentrations) were prepared by mixing 6 mL of 10 ppm pigment in ~ 0.24 N aq HCl. After adjusting the pH to 11 and 2.4 with dropwise addition of 1 N NaOH, 20 mL of 47 µM PAR (final concentration) in 100% methanol was added and the volume was adjusted to 50 mL with Milli-Q water. The ESI mass spectra shown in Figure 2.7 reveal that at high pH the mass spectra are very noisy but the $[Fe^{III}(PAR)_2]^+$ ion is visible above the noise at m/z 484 (Figure 2.7B). At low pH, the mass spectra exhibit little noise, and the intensity of the M^+ ion of $[Fe^{III}(PAR)_2]^+$ is very high relative to the background (Figure 2.7D). Upon binding to Fe^{III}, the ortho hydroxyl group of the resorcinol ring (Table 2.4) is deprotonated so that

each ligand carries a single negative charge giving rise to an overall +1 charge for the [$Fe^{III}(PAR)_2$]$^+$ complex ion. The free PAR ligand is poorly ionized compared to the complex ion under the experimental conditions used as evidenced by the low intensity of its MH$^+$ ion at m/z 216 (Figure 2.7D). This is advantageous because excess free ligand will not suppress the signal of the complex ion at m/z 484. Since the PAR complex of iron at low pH also produces a more intense MH$^+$ ion relative to the PAN complex (Figure 2.6D vs 2.7D), PAR was selected as a suitable ligand for further ESI-MS work.
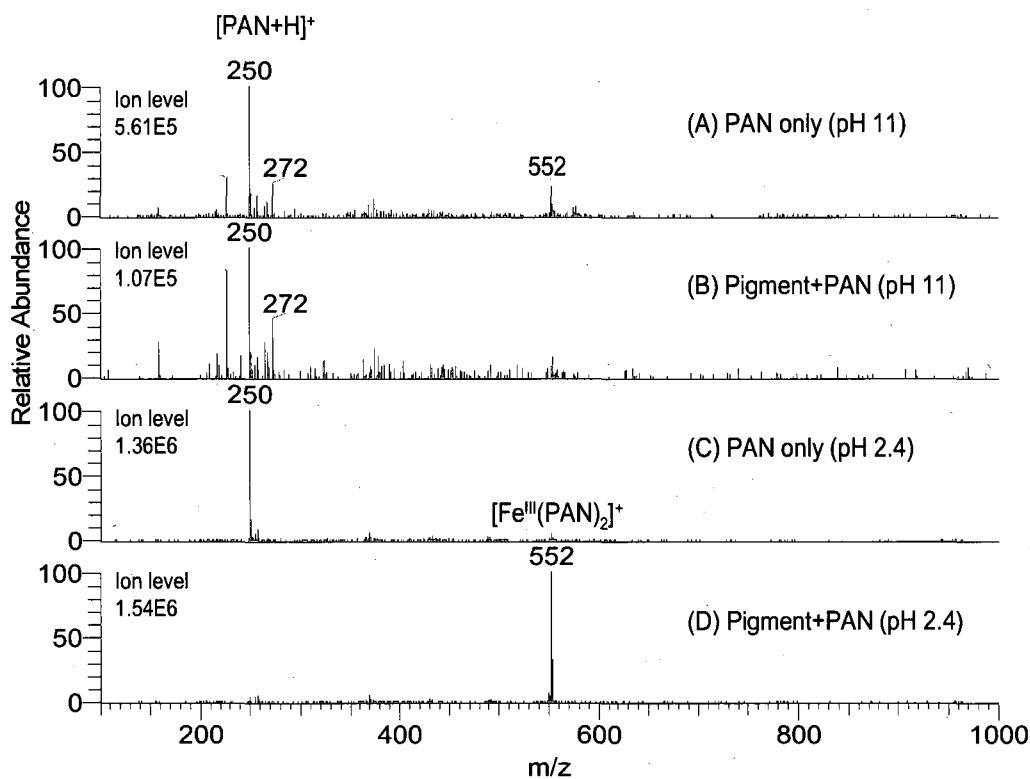
Figure 2.6: ESI mass spectra of solutions containing 7.5 µM pigment-derived iron and 16 µM PAN in 40% aq methanol. The iron solution was prepared by mixing 6 mL of 10 ppm pigment in ~ 0.24 N aq HCl with 20 mL of 40 µM PAN in 100% methanol, and diluting to 50 mL with Milli-Q water after pH adjustment. A 50-µL sample aliquot was directly injected with the mobile phase (50% aq methanol/0.1% formic acid) at a flow rate of 1 mL/min and split at 120 µL/min to ion source. The heated capillary temperature was set at 350°C. The mass spectrum was obtained with a 1-min scan time, and each scan was set at 50 ms.
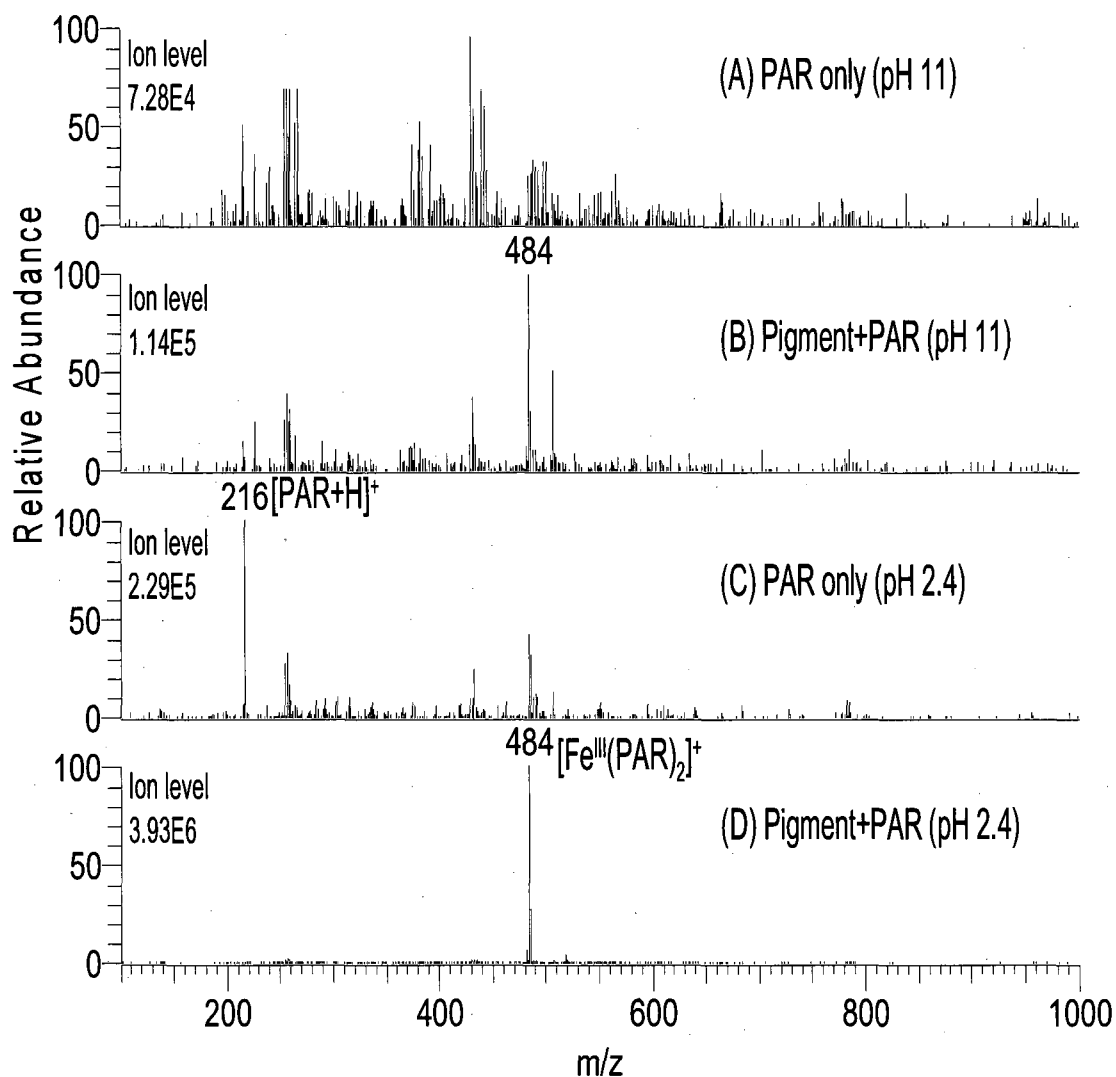
Figure 2.7: ESI mass spectra of solutions containing 7.5 μM pigment-derived iron and 19 μM PAR in 40% aq methanol. The iron solution was prepared by mixing 6 mL of 10 ppm pigment in ~ 0.24 N aq HCl with 20 mL of 47 μM PAR in 100% methanol, and diluting to 50 mL with Milli-Q water after pH adjustment. A 50-μL sample aliquot was directly injected with the mobile phase (50% aq methanol/0.1% formic acid) at a flow rate of 1 mL/min and split at 120 μL/min to ion source. The heated capillary temperature was set at 350°C. The mass spectrum was obtained with a 1-min scan time, and each scan was set at 50 ms.

2.3.4 Confirmation of $[Fe^{III}(PAR)_2]^+$ identity by isotope distribution analysis

A zoom scan was performed on the LCQ Deca to record the isotope pattern of the $[Fe^{III}(PAR)_2]^+$ complex at m/z 484. The empirical formula of the complex $(FeC_{22}H_{16}N_6O_4)$ was entered into an isotope calculator [27], which calculated the relative abundance of the peaks arising from the isotopes. The theoretical isotope pattern (Figure 2.8 inset) matches that observed for the m/z 484 ion shown as a zoom scan in Figure 2.8. A comparison of the relative abundance of the isotope peaks in the theoretical and experimental spectra (Table 2.5) confirms that a single iron atom is present in the m/z 484 ion.
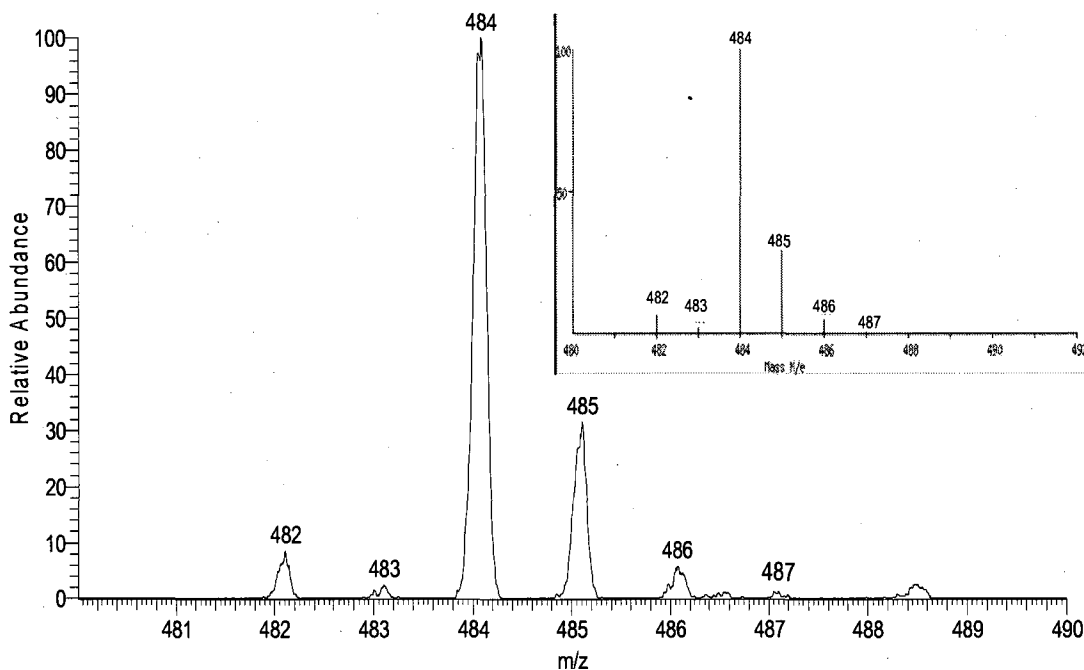
Figure 2.8: Zoom scan of the MH$^+$ ion of the [Fe^{III}(PAR)$_2$]$^+$ complex and its theoretical mass spectrum (inset). The experimental conditions are given in the legend of Figure 2.7. The zoomed scan was performed at 50 ms/scan.

Table 2.5: Comparison of the theoretical and experimental isotope peak intensities for $FeC_{22}H_{16}N_6O_4$

m/z	Relative abundance	
	Theoretical[a]	Experimental[b]
482	6.2	8.0
483	1.6	2.0
484	100.0	100.0
485	28.6	30.0
486	5.0	6.0
487	0.6	1.0

[a] Calculated using the isotopic calculator in Ref [27].

[b] Peak heights from zoom scan in Figure 2.8.

2.4 Quantitative analysis of total iron

In order to ensure the acceptability of a method for quantitative analysis, certain specifications need to be met. These are defined by the US FDA in their guidelines for industry [28, 29]. The bioanalytical method validation criteria were adopted here because of their relevance for the current analysis process and sample preparation procedures. The FDA requires that every sample determination include a calibration curve and quality control checks, and acknowledges that most current bioanalytical methods use mass spectrometry. The need for a calibration curve is because of the inherent variability in the processing of each sample, in extraction recovery, and from signal variation in the instrumentation. It should also be emphasized that the FDA guidelines are used as a foundation for establishing quantitative analytical methods for the determination of an active pharmaceutical ingredient (API). Specifications for the quantitative analysis of an

API are usually more stringent than for pigments [28], and the figures of merit adopted are summarized in Table 2.6.

Quantitative analysis was performed here using the selected-ion monitoring (SIM) mode of the mass spectrometer at m/z 484. In this mode, the sensitivity of detection is enhanced and it is also significantly more selective than full-scan mode. SIM mode is targeted only at the m/z value of the specific ion of interest, and ions at other m/z values will not be detected in the mass spectrometer. Thus, selection of SIM mode will help in attaining the required sensitivity and selectivity (Table 2.6).

Table 2.6: Method validation figures of merit based on US FDA guidelines[a]

Definition	Specification
Limit of Detection (LOD)	Signal-to-Noise ratio (S/N) ≥ 3 or 3xStandard Deviation
Limit of Quantitation (LOQ)	Signal-to-Noise ratio (S/N) ≥ 10 or 10xStandard Deviation
Correlation coefficient (R^2)	≥ 0.99
Precision (%RSD) & Accuracy (%Diff)	$\pm 20\%$ at LOQ, $\pm 15\%$ at level $>$ LOQ
Recovery	$\pm 20\%$ at LOQ, $\pm 15\%$ at level $>$ LOQ
Specificity	Signal-to-Interference ratio ≥ 5
Stability	Demonstrate stability
Robustness	Meet precision and accuracy for intra- and inter-day analyses

[a] Specifications are extracted from the US FDA guidelines for bioanalytical method validation [28]

2.4.1 Figures of merit using the LCQ ion trap mass spectrometer

Standards containing 2 to 71 µM of iron were analyzed with the ion trap mass spectrometer. The calibration curve and regression analysis (Figure 2.9) reveal that a linear relationship was obtained with correlation coefficient > 0.99 when the peak intensity at m/z 484 was plotted versus concentration up to 43 µM iron. At higher concentrations, the TIC levelled off for the reason described in Chapter 3. Figure 2.9 also shows two lines; the blue line represents the calibration line without correction for background interference, the red line represents the corrected line. The offset in the two lines reflects a background interference in the analysis of ~ 6%. Following this finding, investigation of the sources of interference (Section 2.4.2) was performed. Use of appropriate labware as well as efficient cleaning protocols for the labware and instrumentation were implemented in future analyses.
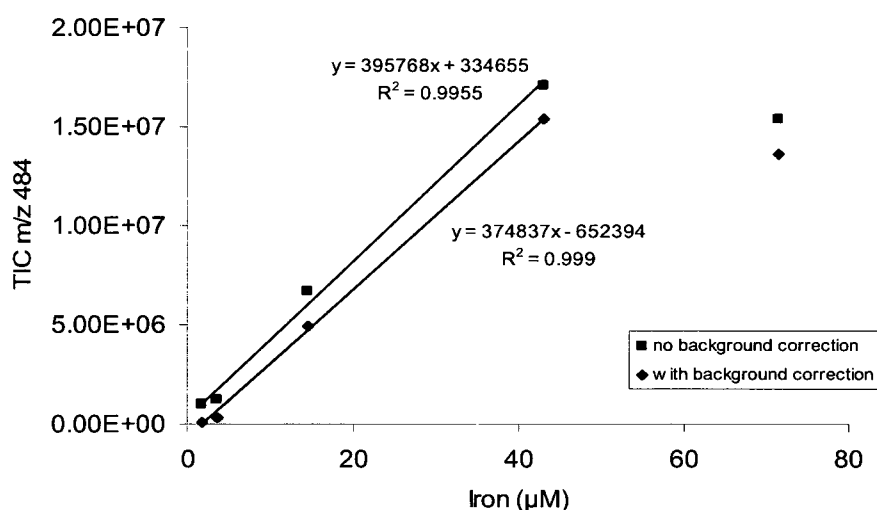
Figure 2.9: Total iron calibration curve using the LCQ ion trap mass spectrometer.
50 µL of the Fe standards were directly injected with the mobile phase (50% aq methanol/0.1% formic acid) at a flow rate of 1 mL/min and split to 120 µL/min to ion source. The heated capillary temperature set at 350°C.

Table 2.7 summarizes the results for the quality control (Qc) sample using the regression-line equation from Figure 2.9. Both precision (1.88% and 1.98% without and with correction) and accuracy (-5.2% and -4.6% without and with correction) meet the acceptance criteria according to the US FDA guidelines. However, the corrected and non-corrected values showed a negative bias indicating that the concentrations used were close to the limit of the dynamic range of the instrument. This bias is also revealed in the negative y-intercept for the corrected curve. From standard deviation, the LOD and LOQ were calculated to be 2 and 8 μM Fe, respectively (Table 2.7).

2.4.2   Interference minimization

Following identification of the appropriate ligand for the complexation, optimization of the reaction conditions were further pursued. As seen in Figures 2.6A, 2.6C, and 2.7C, the matrix blanks exhibit peaks at m/z 552 (for PAN) and m/z 484 (for PAR) due to trace iron impurities in the reagents (HCl, methanol, and formic acid), instrumentation, and labware used in the analysis. Background interference was also seen in the calibration curve generated using the ion trap mass spectrometer (Figure 2.9). Iron impurity is unavoidable, but it can be subtracted if kept constant. Thus, the same reagents and instrumentation were used throughout the sample preparation so that the labware were the main variable source of iron. The interference from the labware following different washing procedures was evaluated by measuring the matrix blank containing PAR. The washing procedures were adopted from an article by Gardner and Carey [30], and the total ion current was measured with the ion trap operating in SIM mode at the m/z value (484) of $[Fe^{III}(PAR)_2]^+$ (Figure 2.7D).

Table 2.7: Figures of merit for method validation using the LCQ ion trap mass spectrometer

Aliquot #	Theoretical concentration 42.86 µM Fe[a]			
	Accuracy (µM)[b] Without correction	%Difference[c]	Accuracy (µM)[d] With correction	%Difference[e]
1	40.3	-5.9	40.6	-5.4
2	40.1	-6.5	40.3	-6.0
3	41.4	-3.5	41.6	-2.9
4	40.6	-5.3	40.8	-4.8
5	42.1	-1.8	42.4	-1.0
6	39.8	-7.1	40.0	-6.6
7	40.6	-5.3	40.8	-4.8
8	40.1	-6.5	40.3	-6.0
9	41.4	-3.5	41.6	-2.9
10	39.6	-7.6	39.8	-7.2
11	41.1	-4.1	41.4	-3.5
Mean	40.6	-5.2	40.9	-4.6
SD	0.76		0.81	
%RSD[f]	1.88		1.98	
LOD[g]	2.28		2.43	
LOQ[h]	7.6		8.1	

[a] Target concentration of Qc sample. [b] Experimental results obtained using the calibration curve without background correction. [c] (Experimental–Target)/Target x 100, using the calibration curve without background correction. [d] Experimental results obtained using the calibration curve with background correction. [e] (Experimental–Target)/Target x 100, using the calibration curve with background correction. [f] %RSD = SD/Mean x 100. [g] LOD calculated from the standard deviation (SD): LOD = 3xSD. [h] LOQ = 10xSD

From the results in Table 2.8, it is obvious that use of polycarbonate-based flasks from Nalgene, which have been washed by the company's procedure (Section 2.2.3) and rinsed with HCl, produces the lowest background interference. Following this finding, polycarbonate-based flasks were used in all future analyses.

Since the HPLC system used in this thesis was not designed for elemental analysis, some of the plumbing consisted of metal-based tubing. Such tubing could contribute to trace iron interference, so critical tubing in the flow path was replaced with polymer-based PEEK® tubing. The stainless steel capillary tubing connecting the HPLC pump to the autosampler injector, the autosampler injector to the ion source of the mass spectrometer, and in the flow splitter was also replaced with PEEK® tubing (Figure 2.10). Furthermore, prior to analysis, the system was flushed with 50% aq methanol/1% CH_3COOH, followed by 50% aq methanol. Replumbing of the triple quadrupole mass spectrometer was also performed to increase of the dynamic range of the calibration curve following analysis of the ion trap data (Section 2.4.1). The efforts made to increase the dynamic range of the triple quadrupole mass spectrometer are described in Chapter 3.

Table 2.8: Trace iron impurity in the labware

TIC (xE5) at m/z 484[a]						
Nalgene flasks[b]				Glass flasks[b]		
HCl[c] wash	HNO$_3$[c] wash	Company wash only[c]	No wash[d]	HCl[c] wash	HNO$_3$[c] wash	Company[c] wash only
1.75	3.59	2.48	4.80	5.64	6.14	5.06

[a] Total ion current (TIC) was recorded in SIM mode at m/z 484 using a LCQ ion trap mass spectrometer (n=1). A 50-µL sample aliquot was directly injected with the mobile phase (50% aq methanol/0.1% formic acid) at a flow rate of 1 mL/min and split at 120 µL/min to ion source. The heated capillary temperature was set at 350°C. [b] 50-mL Nalgene (polycarbonate) volumetric flasks or 50-mL glass volumetric flasks. [c] Flasks were washed using the company's procedure (Section 2.2.3) and then rinsed 3x (where indicated) with 10% acid. [d] New Nalgene flasks were used as received from the manufacturer. Note: no new glassware was purchased and all glassware had already been washed using the company's procedure (Section 2.2.3).

2.4.3 Figures of merit using the triple quadrupole mass spectrometer

To increase the sensitivity of detection as well as dynamic range of the calibration curve, analyses were performed on a triple quadrupole mass spectrometer. A triple quadrupole mass spectrometer differs from an ion trap mass spectrometer in that the transmission of ions occurs linearly, which enhances detection at a given m/z value and is expected to cover a wider dynamic range.

When plotting the TIC peak area in SIM mode at m/z 484 vs concentration, a linear correlation was found from 2 µM to 43 µM total iron (Figure 2.11). Surprisingly, this dynamic range is similar to that obtained with ion trap mass spectrometer, and further investigations are described in Chapter 3.
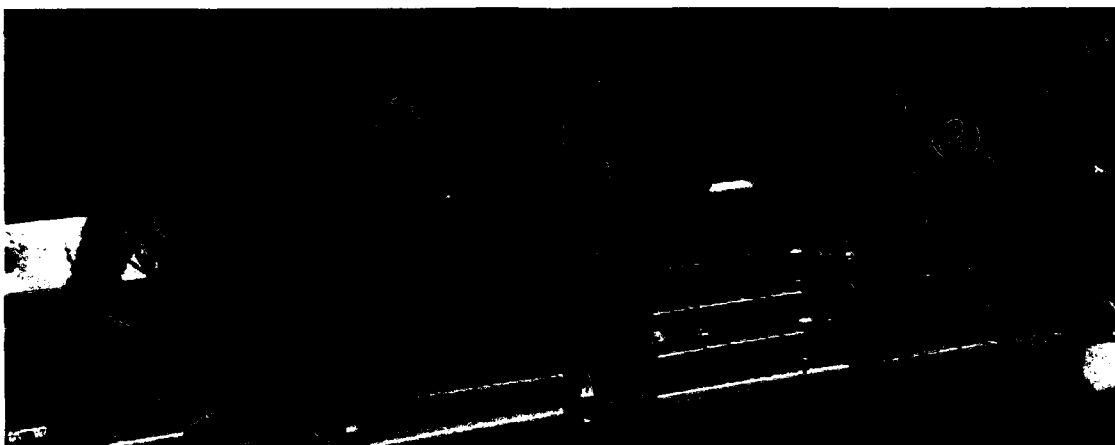
Figure 2.10: Instrument replumbing with PEEK® tubing. Stainless steel capillary tubing (1) from the HPLC pump to the autosampler injector (1.5 mm OD, 0.2 mm ID), (2) from the autosampler injector to the ion source of the mass spectrometer (1.5 mm OD, 0.1 mm ID) and (3) in the flow splitter.

Figure 2.11 also shows that the calibration lines, corrected and not corrected for background interference, are practically superimposable. This further indicates that the cleaning and plumbing procedures minimized background interference (Figure 2.11 vs Figure 2.9).

The LOD (2 μM) is the same as that obtained using the ion trap instrument, but in this case, the LOQ is equal to LOD. Since trace iron impurity is unavoidable, it is more

meaningful to use a signal-to-interference ratio than a S/N. With the LOQ at 2 μM, the

S/N calculated by Xcalibur, the instrument's software, was determined to be 100. Thus,

technically, the LOQ could be pushed 10-fold lower to meet 10 x S/N, but this would

result in iron over-estimation due to the background interference. With the LOQ at 2 μM,

the signal-to-interference ratio was determined to be > 5 (Figure 2.12). This ratio meets

FDA guidances which requires that the lowest standard concentration in the calibration

curve (i.e., the LOQ) exhibit a response that is $\geq$ 5-fold higher than that of the blank

(Table 2.6) [29]. Figure 2.12 also shows that the method specificity criterion is met, since

it clearly indicates that the LOQ signal is greater than the blank signal.
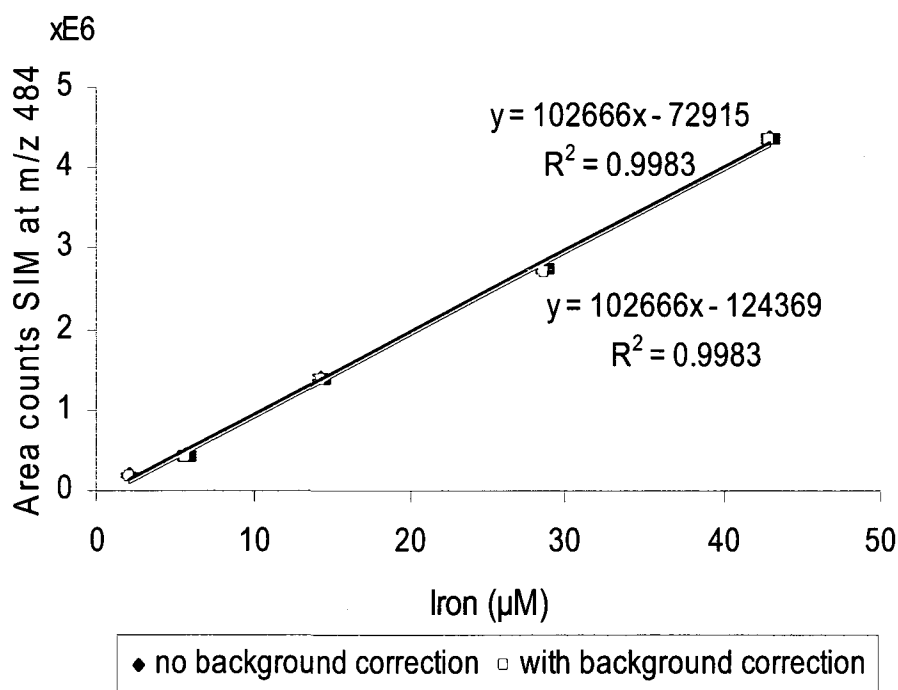
Figure 2.11: Total iron calibration curve obtained on the triple quadrupole mass spectrometer. A 50-μL sample aliquot was directly injected with the mobile phase (50% aq acetonitrile/0.1% formic acid) at a flow rate of 1 mL/min and split at 120 μL/min to ion source. The heated capillary temperature was set at 350°C.
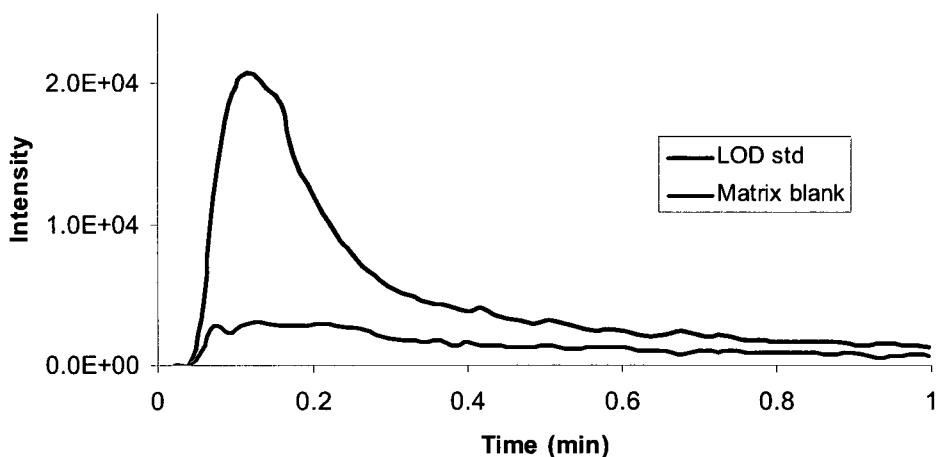
Figure 2.12: Overlay ESI MS TICs of matrix blank and LOD standard. See experimental details in the legend of Figure 2.11.

Method repeatability or robustness was tested by preparing intraday and interday quality control (Qc) samples. Intraday Qc samples were processed on the same day as the calibration standards while the interday Qc samples were processed the day after the standards and the intraday Qc samples. The Qc samples were targeted at two levels within the linear range of the calibration curve, one at $\sim 3x$ the lowest concentration and the other at 80% of the highest concentration. The intraday analysis involved duplicate Qc preparation at each concentration, whereas single replicates were prepared for the interday analysis. Triplicate measurements were recorded for each Qc sample and each calibration standard. The means of the signal from the total area of the TIC peaks at m/z 484 were plotted against iron concentration. The ranges, which indicate the minimum and the maximum signal obtained from the triplicate measurements, are indicated by the y-error bars in Figure 2.13. The results (Table 2.9) show that repeatability was established since all Qc values are within the accepted criteria for precision and accuracy listed in Table 2.6.

Figure 2.13 reveals that the standards were stable for at least two days when stored under ambient laboratory conditions. The results obtained using the 2-day calibration curve are listed in Table 2.9 in the Interday column.
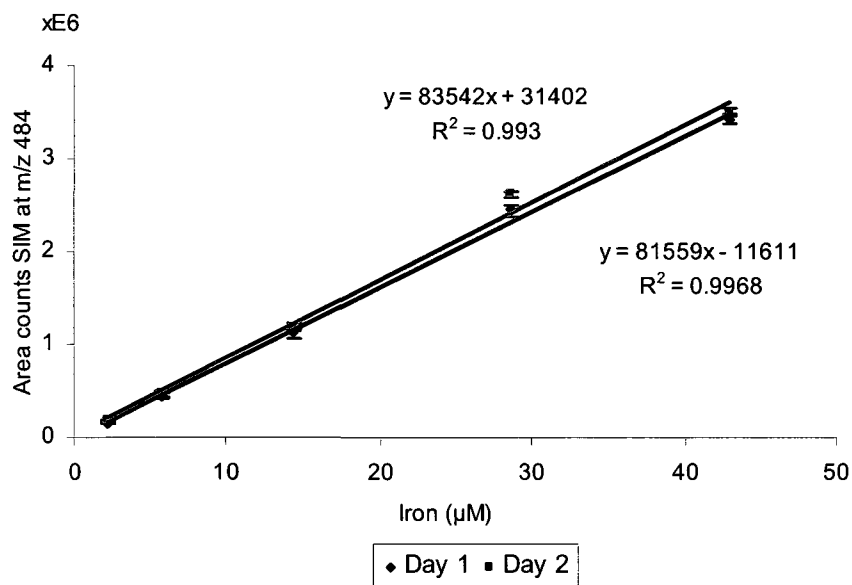
Figure 2.13: Calibration curves obtained using the triple quadrupole mass spectrometer on two consecutive days. Experimental conditions given in the legend of Figure 2.11.

2.4.4 Tablet extraction and iron recovery

Following method optimization and validation using the triple quadrupole mass spectrometer (Section 2.4.3), tablets containing iron oxide pigment were analyzed. Pigment was extracted from red and yellow film-coated tablets and also from compressed tablets containing dispersed pigments. Core tablets containing no pigment but with similar formulation to the tablets with pigment were also extracted. To establish its percent recovery, a known amount of iron standard was added to the core tablets and extracted in the same manner as the test tablets.

Table 2.9: Repeatability results for Qc samples obtained using the triple quadrupole mass spectrometer[a]

Intraday			Interday		
Qc (µM)[b]	Observed (µM)	%Difference[c]	Qc (µM)[b]	Observed (µM)	%Difference[c]
Low#1 (7.14)	6.83	-4.30	Low#3 (7.14)	7.04	-1.38
	7.08	-0.78		7.04	-1.41
	7.11	-0.45		7.08	-0.88
Low#2 (7.14)	7.56	5.94	**Mean**	**7.05**	**-1.23**
	7.57	6.07	**%RSD[d]**	**0.30**	
	7.66	7.28			
Mean	**7.30**	**2.29**			
%RSD[d]	**4.65**				
High#1 (35.7)	33.9	-4.98	High#3 (35.7)	37.6	5.28
	34.2	-4.36		37.4	4.76
	34.3	-4.07		37.5	4.93
High#2 (35.7)	37.8	5.74	**Mean**	**37.5**	**4.99**
	37.1	3.94	**%RSD[d]**	**0.25**	
	36.6	2.59			
Mean	**35.6**	**-0.19**			
%RSD[d]	**4.81**				

[a] Data obtained as outlined in the legend of Figure 2.11. [b] Qc is a quality control sample of known target concentration to check for accuracy. [c] (Observed-Target)/Target x 100. [d] Standard deviation/Mean x 100.

Table 2.10 compares the total iron found in the tablets with the expected amounts. The percent iron oxide in the pigment mixture was not revealed by the supplier so the pigment was assumed to contain 55% iron oxide, the maximum allowed by the FDA (Chapter 1). The recovery of the iron added to the core tablets was found to be 93% and assuming 55% iron oxide in the pigments, the recovery of iron oxide from the test tablets is within the specification listed in Table 2.6 ($\pm$ 20%) except for the red film-coated tablets. It should also be emphasized that the pigment uniformity, unlike API uniformity, was never optimized in the tablets. In addition, different pigment was used in each tablet type in Table 2.10. Importantly, 93% recovery from the spiked standard indicates that the extraction process is efficient.

Table 2.10: Total iron concentrations from extracted tablets[a]

Tablet type	Observed [Fe][b], μM	Expected [Fe][c], μM	% Recovery[d]
Yellow FCT[e]	8.42 ± 0.05	9.13	92.2
Red FCT[e]	6.94 ± 0.07	9.19	75.5
Yellow OCT[f]	18.6 ± 0.10	21.73	85.6
Core	< LOD	0	N/A
Core + standard	2.65 ± 0.01	2.86	92.7

[a] Tablets extracted as described in Section 2.2.5. [b] Average experimental results reported from n=2. [c] Expected concentration assuming 55% iron oxide in pigment. [d] Observed/Expected x 100. [e] Film-coated tablet. [f] Oral compressed tablet. Experimental details are given in the legend of Figure 2.11.

2.4.5 Comparison of ICP-OES and ESI-MS results

ICP-OES analyses were performed to confirm the applicability of the ESI-MS method for in-process testing of tablets containing iron oxide pigment. It should be noted that complexation is not required to quantitate iron by ICP-OES. The values obtained by ESI-MS (Table 2.10) were plotted against those obtained by ICP-OES and a good correlation ($R^2 \geq 0.99$) was obtained (Figure 2.14). This approach for comparing two different methods was adopted from De and Roberts [31]. In addition, the Student's t-test was performed and the results are given in Table 2.11. The paired-t test value was determined using a calculator available on the web [32]. The threshold p-value is set at 0.05 and a p-value greater than the threshold indicates that the difference is not statistically significant. Based on the correlation coefficient (0.9955) and p-value obtained here (0.1378), the ESI-MS and ICP-OES results are not statistically different. Thus, the ESI-MS method developed here is comparable in performance to ICP-OES, and can be adopted for total iron analysis in tablets containing iron oxide pigment.
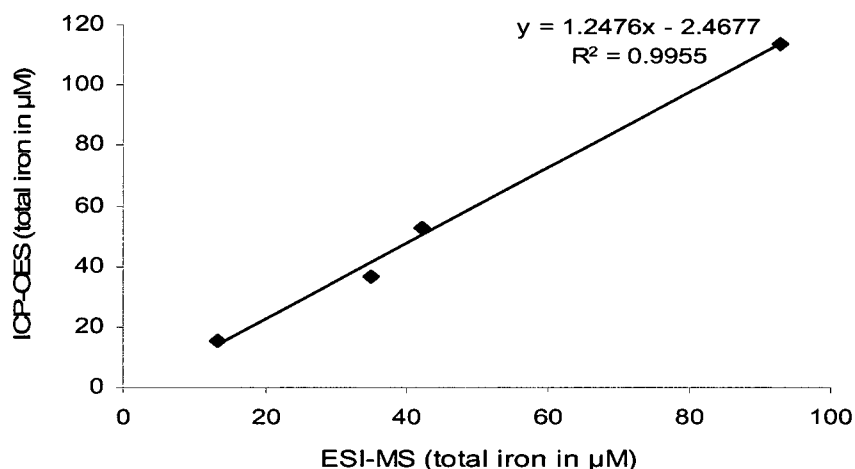
Figure 2.14: Comparison of total iron analysis by ESI-MS and ICP-OES. Data taken from Table 2.11.

Table 2.11: Statistical comparison of iron analysis by ESI-MS and ICP-OES

Tablet	[Fe] (µM) ESI-MS[a]	[Fe] (µM) ICP-OES[b]
Yellow FCT[c]	42.1	52.7
Red FCT[c]	34.7	36.9
Yellow OCT[d]	92.8	113.4
Core + standard	13.3	15.3
Mean	45.725	54.575
SD	33.676	42.106
Correlation coefficient R^2	0.9955	
Student t-test p value	0.1378	

[a] Results obtained by ESI-MS are from Table 2.10 taking the 5x dilution factor into account since working solutions for ICP-OES were 5x more concentrated than those used in ESI-MS. Samples for ICP-OES were aspirated into the system directly without any further additional preparation prior to the last dilution step when PAR was added (Section 2.2.5). [b] ICP-OES conditions: nebulizer gas was argon, sample flush time was 30 s, and the plasma was generated using RF power of 1150W. The nebulizer flow was 0.7 L/min and the auxiliary gas flow 0.5 L/min. The 259.9-nm emission line was used for detection of iron. [c] Film-coated tablet. [d] Oral compressed tablet.

Chapter 3   Characterization of the iron-PAR complexes

3.1   Introduction

In Section 2.4.1, it was noted that the calibration curve generated using the LCQ ion trap mass spectrometer levelled-off at 43 μM iron (Figure 2.9). This behaviour was not unexpected because ion transmission from the ion trap to the detector is not linear. Further analysis was carried out on a triple-quadrupole mass spectrometer, which is expected to exhibit an increased linear range compared to the ion trap mass spectrometer. Using the same heated capillary temperature, spray voltage, LC mobile-phase composition, mobile-phase flow-rate, split ratio to the ion source, the calibration range increased from 43 μM on the LCQ to 86 μM on the TSQ. The LOQ remained the same, being ~ 2 μM.

In addition, the Fe-PAR calibration standards exhibited a linear relationship with the $R^2 \geq 0.99$ on both day 1 and day 2. However, the slope of calibration line decreased over time as shown in Figure 3.1, which suggested that the standards were unstable. At first thought, the levelling-off of the calibration curve at higher iron concentration and the decreasing slope of the calibration line with time were attributed to insufficient PAR despite the fact that the ligand was 35% in excess (233 μM) relative to the highest iron concentration (86 μM) assuming formation of the $[Fe^{III}(PAR)_2]^+$ bis complex. As a result, further investigations into these issues were warranted.

3.2 Effects of increasing PAR concentration

An Fe^{III} standard was prepared from the commercial stock (1000 ppm Fe^{III}, Ricca Chemical Co, TX, USA) by dilution with Milli-Q water. Rather than preparing a range of calibration standards, the highest iron concentration (86 µM) within the dynamic range (Figure 3.1) was examined. A 2.23 mM PAR stock solution was prepared in 100% methanol and added to the 86 µM Fe^{III} standard in water (pH ~3). Spectra were recorded in a 0.2-cm cuvette over a 24-h period at different PAR concentrations (Figure 3.2). The sample containing 10% methanol was only monitored over a 2-h period due to the formation of a precipitate within 30 min. The absorbance at 530 nm, which is the visible maximum of the $[Fe^{III}(PAR)_2]^+$ complex, was recorded.
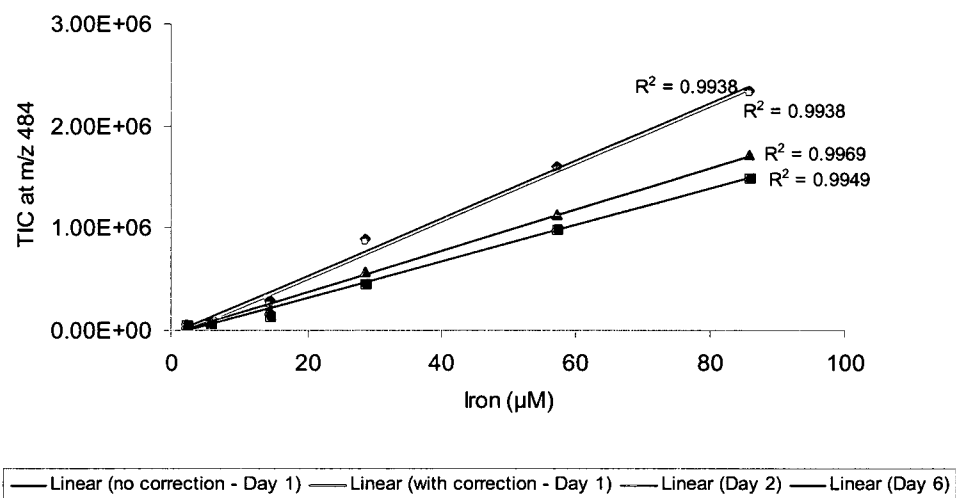
Figure 3.1: Iron calibration plots using the triple quadrupole mass spectrometer over a period of 6 days with 233 µM PAR. A 50-µL aliquot of each standard was directly injected with the mobile phase (50% aq methanol/0.1% formic acid) at a flow rate of 1 mL/min and split at 120 µL/min to ion source. The heated capillary temperature was set at 350°C. The iron standards were prepared from the commercial stock solution as described in Section 2.2.4.
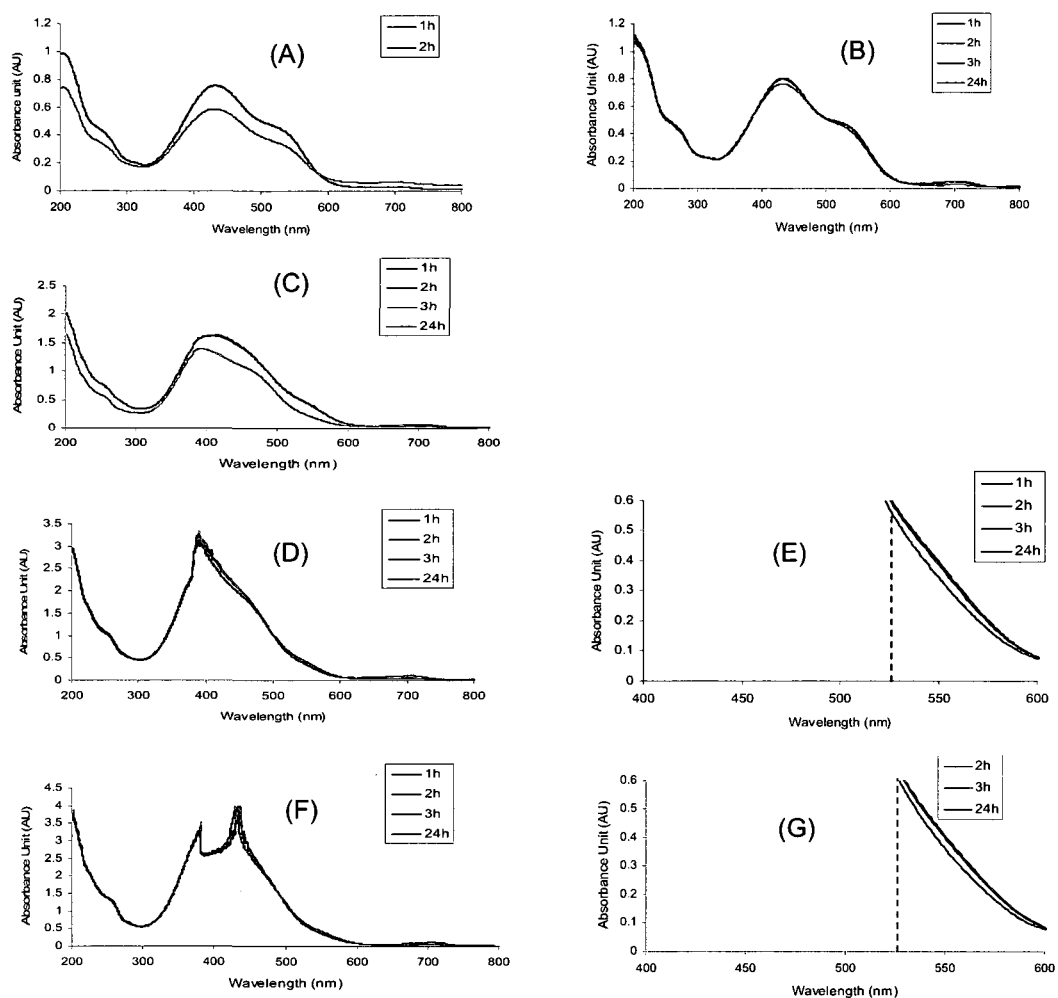
Figure 3.2: Changes in the UV-Vis spectra of iron-PAR solutions over time vs PAR concentration. Spectra were recorded in a 0.2-cm cuvette. The aqueous solutions contained 86 μM Fe^{III} standard and the following PAR and methanol concentrations: (A) 223 μM PAR and 10% methanol; (B) 223 μM PAR and 40% methanol; (C) 446 μM PAR and 20% methanol; (D) 669 μM PAR and 30% methanol; (E) Same as (D) but zoomed 10x from 400 nm to 600 nm; (F) 892 μM PAR and 40% methanol; (G) Same as (F) but zoomed 10x from 400 nm to 600 nm.

From the results in Table 3.1, it appears that a minimum of 40% methanol is required to prevent precipitation in the iron/PAR solution. Also, regardless of the amount of excess PAR in the solution, the 530-nm absorbance decreases over 30 min (10% methanol) to 24 h (Table 3.1). The composition of the precipitates was not investigated,

but it is suspected that the free PAR ligand has low solubility in a highly aqueous environment at the pH of the experiment (~3). The PAR used in this experiment was in the free base form, rather than the salt form that is commonly used in the literature for colorimetric analysis [33-35]. The structure of the free acid (protonated form) is shown in Table 2.4. The salt form is highly soluble in water, whereas the free base form is soluble in organic media [21]. Nevertheless, with 40% methanol content in the sample solution, insufficient ligand was not the cause of the issues discussed in Section 3.1.

Table 3.1: Stability of iron-PAR complexation vs excess PAR [a]

% methanol	[Fe], μM	[PAR], μM	% excess PAR [b]	Precipitate	Δ530nm (%)
10	86	223	30	✓	> 10
20	86	446	150	✓	> 10
30	86	669	290	✓	< 10
40	86	892	420	✗	< 10
40	86	223	30	✗	< 10

[a] Solutions of 86 μM Fe^{III} standard containing the PAR and methanol concentrations indicated were prepared at room temperature. Spectra were recorded in a 0.2-cm cuvette. [b] Percent excess was calculated based on two mole equivalents of PAR for each mole [Fe].

3.3 Effects of organic solvent on stability of iron-PAR complexes

PAR was dissolved in 100% methanol or 100% acetonitrile and added to 86 μM of Fe^{III} standard or Fe^{II} in water at pH ~3. The latter was prepared using $FeSO_4$ as source of ferrous iron, and the total organic content of the sample solutions was adjusted to 40%. Evaluation of sample stability was performed visually by comparing the color of the solution over a one-week period, and a summary of the findings is given Table 3.2.

Table 3.2: Color formation in Fe/PAR solutions[a]

	$[Fe^{III}(PAR)_2]^+$ preparation			$[Fe^{II}(PAR)_2]$ preparation		
Solvent	Color initial	Color after 1wk	Precipitate[b]	Color initial	Color after 1wk	Precipitate[b]
40% aq methanol	Ruby red	Red brown	✗	Red brown	Pale brown	✓
40% aq acetonitrile	Ruby red	Ruby red	✗	Red brown	Red brown	✗

[a] Solutions containing 86 μM Fe^{III} or 86 μM $FeSO_4$ standard with 233 μM PAR in the solvent indicated were left standing at ambient laboratory conditions, and the color was visually observed over time. [b] ✗ indicates that no precipitate was observed and ✓ indicates that a precipitate was observed.

The initial color of the Fe^{III} and Fe^{II} complexes in 40% acetonitrile did not change over a period of one week, while in 40% methanol the color changed from ruby red to red-brown (Table 3.2). Formation of a red-brown color suggested possible Fe^{III} reduction in methanol. Thus, an HPLC method was developed using a diode-array detector to separate the Fe^{III} and Fe^{II} PAR complexes before their introduction into the ESI source of the mass spectrometer. Separation of the $[Fe^{III}(PAR)_2]^+$ and $[Fe^{II}(PAR)_2]$ complexes and their relative retention times on the HPLC column can be seen in Figure 3.3. An overlay of the spectra recorded on the diode-array detector reveals that the Fe^{II} and Fe^{III} complexes have isosbestic points at 396 nm and 505 nm (Figure 3.4). Table 3.2 shows that the formation of $[Fe^{II}(PAR)_2]$ was slower in acetonitrile. Thus, this solvent was used to replace methanol in further analyses.
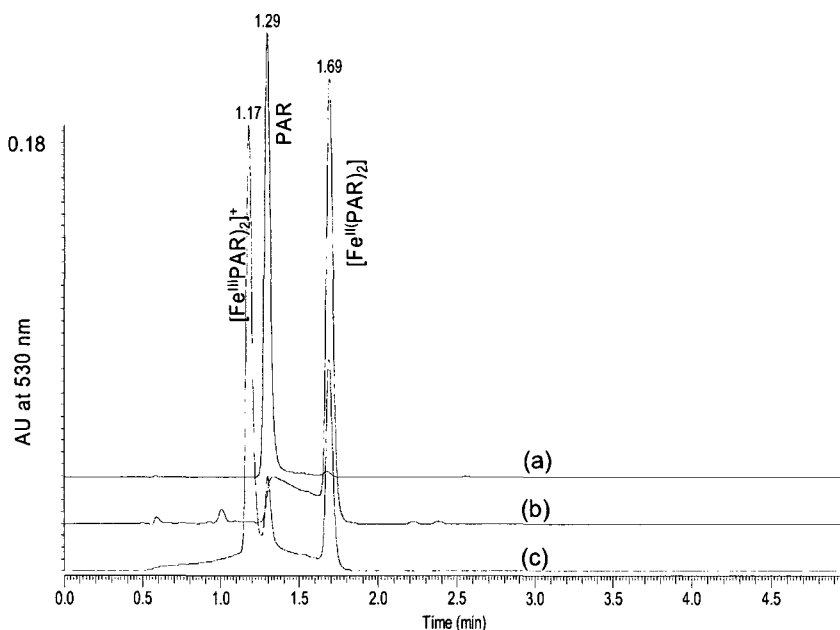
Figure 3.3: Overlay of HPLC-Vis (530 nm) chromatograms of solutions of PAR, [Fe^{III}(PAR)$_2$]$^+$, and [Fe^{II}(PAR)$_2$]. A 5-μL aliquot of a freshly prepared solution in 40% aq acetonitrile of (a) 223 μM PAR, (b) 86 μM FeSO$_4$ with 223 μM PAR, (c) 86 μM Fe^{III} standard with 223 μM PAR was injected onto an Agilent Technologies, Eclipse Plus C18 RRHT column (50 x 4.6 mm, 1.8 μm particle size at 40°C). The mobile phase (30% aq 0.05% TFA in acetonitrile) was pumped at a flow rate of 1 mL/min through HPLC system equipped with a diode-array detector set at 530 nm. The total run time was 5 min.
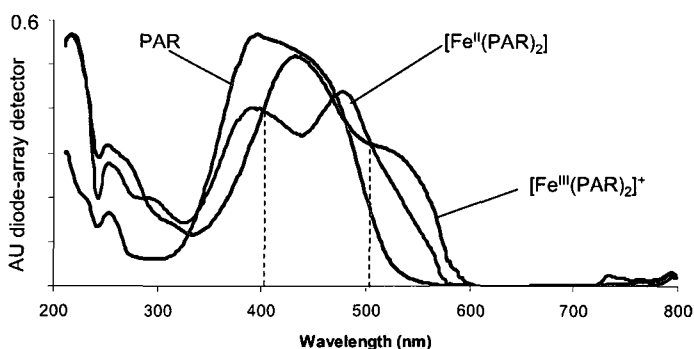
Figure 3.4: Overlay of UV-Vis Spectra of PAR, [Fe^{III}(PAR)$_2$]$^+$ and [Fe^{II}(PAR)$_2$] complexes. Spectra were recorded using the diode-array detector during the HPLC analysis described in Figure 3.3. The Fe^{II} and Fe^{III} complexes exhibit isosbestic points at 404 nm and 505 nm (dashed lines).

3.4 Reduction of Fe^{III} upon addition of PAR

Representative HPLC chromatograms of standards containing 223 µM PAR and 57 µM or 86 µM Fe^{III} standard in 40% aq acetonitrile are shown in Figure 3.5. The eluate was monitored at 400 nm, which is close to the isosbestic point of the Fe^{II} and Fe^{III} complexes (Figure 3.4) and it is also the highest UV wavelength absorption setting available using the variable-wavelength detector. Free PAR was well resolved from its complexes (Figure 3.5); hence, its absorbance at 400 nm (Figure 3.4) did not interfere.

The calibration curve shown in Figure 3.6 reveals that a plot of $[Fe^{III}(PAR)_2]^+$ vs peak area at 400 nm is not linear suggesting that $[Fe^{II}(PAR)_2]$ was present in each calibration standard. The sum of $[Fe^{III}(PAR)_2]^+$ and $[Fe^{II}(PAR)_2]$ peak areas vs total iron concentration was linear ($R^2 = 0.9999$) confirming that Fe^{III} was partially reduced when PAR was added since the standards were assayed within 1 h of their preparation. In addition, Figure 3.6 reveals that no Fe^{III} complex was formed at low iron concentration (up to ~ 30 µM) suggesting that Fe^{III} is reduced to Fe^{II} by excess PAR. Products formed on PAR oxidation were not investigated. Yotsuyanagi et al. [23] reported that $[Fe^{II}(PAR)_2]$ is more stable than $[Fe^{III}(PAR)_2]^+$ as is also the case for the Phen complexes. Interestingly, they also found that the $[Co^{III}(PAR)_2]^+$ was more stable than the $[Co^{II}(PAR)_2]$ complex. Oxidation of $[Co^{II}(PAR)_2]$ and reduction of $[Fe^{III}(PAR)_2]^+$ was suspected when solutions of these complexes were introduced from a capillary electrophoresis system into the ESI source of a LCQ-Duo mass spectrometer [36].

The order of addition of reagents, buffering at pH 4, 5, 7, and adding an oxidant (H_2O_2) were investigated to establish their effects on $[Fe^{III}(PAR)_2]^+$ reduction. Jezorek et al. [37] indicated that PAR is light sensitive, so the sample solution was protected from

light during preparation. These modifications did not prevent the reduction of the

$[Fe^{III}(PAR)_2]^+$ complex.
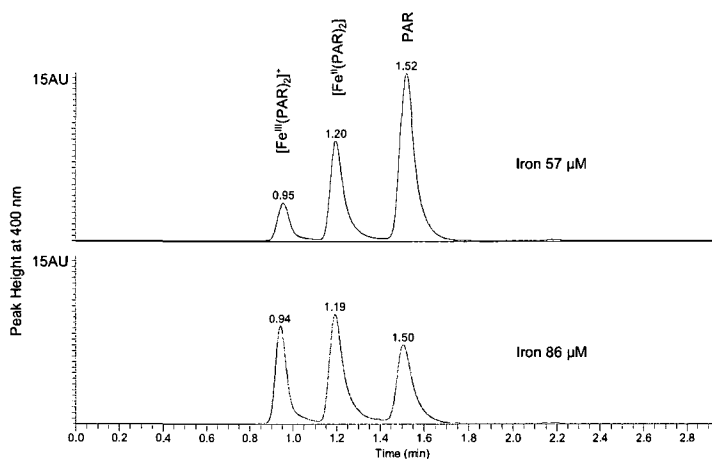
Figure 3.5: HPLC-UV (400 nm) chromatograms of the standard solutions. A 50-µL aliquot of 57 and 86 µM Fe^{III} standard with 223 µM PAR in 40% aq acetonitrile was injected onto an Agilent Technologies, Eclipse Plus C18 RRHT column (50 x 4.6 mm, 1.8 µm particle size at 40°C). The mobile phase (50% aq 0.02% acetic acid/0.01% TFA in acetonitrile) was pumped at a flow rate of 0.6 mL/min through the HPLC system equipped with a variable-wavelength detector set at 400 nm. The total run time was 3 min.
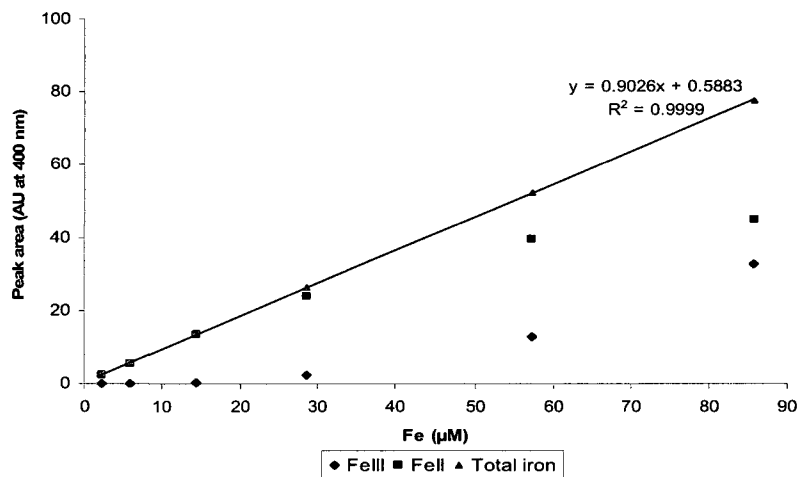
Figure 3.6: HPLC-UV (400 nm) calibration curves for $[Fe^{III}(PAR)_2]^+$, $[Fe^{II}(PAR)_2]$, and total iron. Experimental conditions are given in the legend of Figure 3.5. Calibration standards were assayed 1 h after preparation.

3.5   Addition of reductant

Since the $[Fe^{II}(PAR)_2]$ complex is stable, a reductant was added to fully reduce the complex. Two commonly used reductants are hydroxylamine and ascorbic acid, and their relative efficiencies were monitored by HPLC (Figure 3.7). A trace amount of $[Fe^{III}(PAR)_2]^+$ was detected in the hydroxylamine solution but not in the ascorbic acid solution. Thus, ascorbic acid was selected as the reductant in further analyses. Ascorbic acid acts as a two-electron reductant as shown in equation 3.1 [24, 25]; thus, two moles of Fe^{III} are reduced by one mole of the acid (equation 3.2).
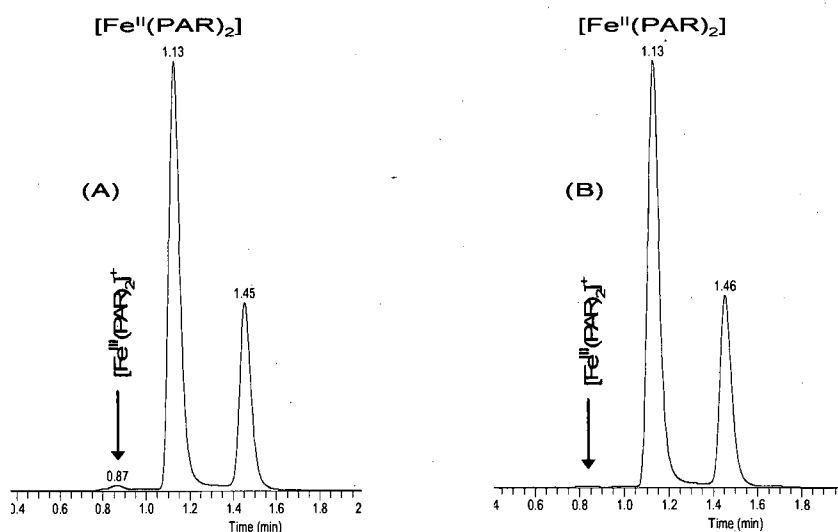
Figure 3.7: HPLC-UV (400 nm) analysis of $[Fe^{III}(PAR)_2]^+$ reduction by (A) 345 μM hydroxylamine and (B) 136 μM ascorbic acid. A 50-μL aliquot of 86 μM Fe^{III} standard with 223 μM PAR in 40% aq acetonitrile was injected onto an Agilent Technologies, Eclipse Plus C18 RRHT column (50 x 4.6 mm, 1.8 μm particle size at 40°C). The mobile phase (50% aq 0.02% acetic acid/0.01% TFA in acetonitrile) was pumped at a flow rate of 0.6 mL/min through the HPLC system equipped with a variable-wavelength detector set at 400 nm. The total run time was 3 min.
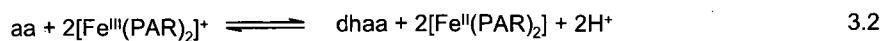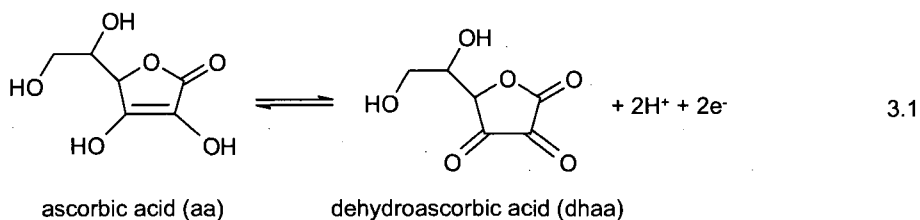
OH ... O=... (structure)

ascorbic acid (aa)   dehydroascorbic acid (dhaa)

$$\text{ascorbic acid (aa)} \rightleftharpoons \text{dehydroascorbic acid (dhaa)} + 2H^+ + 2e^- \qquad 3.1$$

$$aa + 2[Fe^{III}(PAR)_2]^+ \rightleftharpoons dhaa + 2[Fe^{II}(PAR)_2] + 2H^+ \qquad 3.2$$

The ESI mass spectrum of the ascorbate-reduced $[Fe^{II}(PAR)_2]$ complex was recorded and is shown in Figure 3.8. The base peak at m/z 485 corresponds to the protonated bis PAR complex, $[Fe^{II}(PAR)_2+H]^+$.

485.0

* unknown

m/z

Relative Abundance
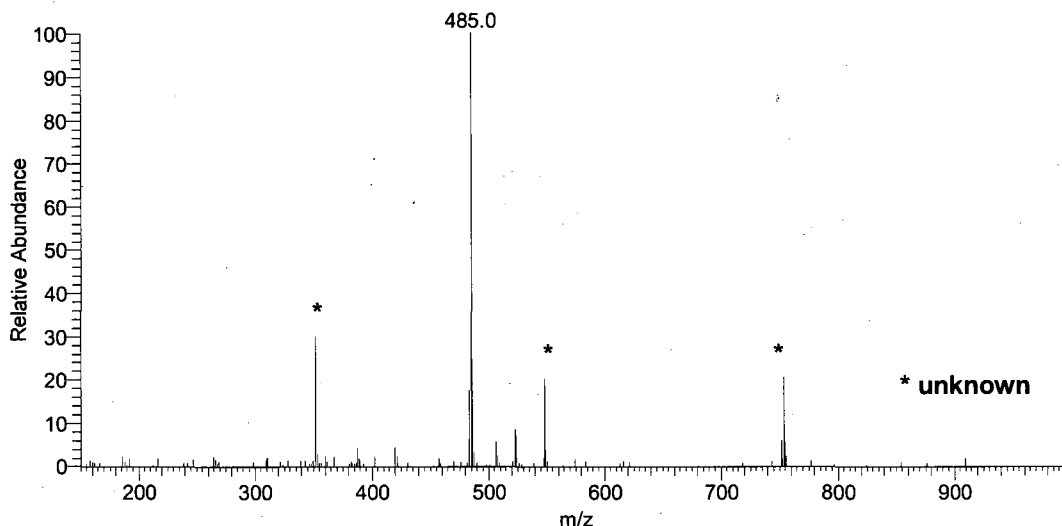
Figure 3 8: ESI mass spectrum of the ascorbate-reduced $[Fe^{II}(PAR)_2]$ complex. A 50-µL aliquot of 86 µM Fe^{III} standard with 223 µM PAR and 136 µM ascorbic acid in 40% aq acetonitrile was directly injected with the mobile phase (50% aq acetonitrile/0.1% formic acid) at a flow rate of 1 mL/min and split at 120 µL/min to ion source. The heated capillary temperature was set at 350°C.

When a solution of $[Fe^{III}(PAR)_2]^+$ in 40% aq methanol was re-examined by LC-MS in SIM mode (m/z 485) after one week, peaks due to both $[^{56}Fe^{II}(PAR)_2+H]^+$ and

$[^{57}Fe^{III}(PAR)_2]^+$ were observed (Figure 3.9). This clearly indicates that these isobaric

species are resolved on the HPLC column using the optimized conditions given in the

legend of Figure 3.9.
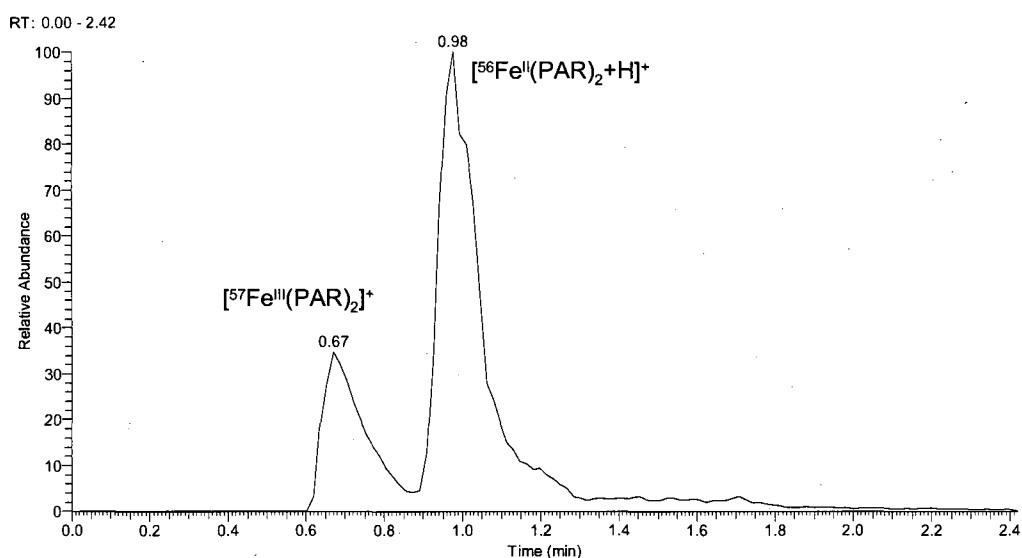
Figure 3.9: LC-MS TIC chromatogram in SIM mode at m/z 485 of a $[Fe^{III}(PAR)_2]^+$ solution after one week. A 10-μL aliquot of 86 μM Fe^{III} standard with 223 μM PAR in 40% aq methanol was injected onto an Agilent Technologies, Eclipse Plus C18 RRHT column (50 x 4.6 mm, 1.8 μm particle size at ambient column temperature). The mobile phase (40% aq 0.02% acetic acid/0.01% TFA in acetonitrile) was pumped at a flow rate of 1 mL/min through the HPLC system and split at 120 μL/min to ion source. The heated capillary temperature was set at 350°C. The total run time was 2.4 min.

The stability of the $[Fe^{II}(PAR)_2]$ complex was examined using the 86 μM Fe^{III}

standard with the reductant (ascorbic acid) at different pH values (1.5, 4, 8, and 10). To

ensure a final solution pH of 1.5, a 0.1-N HCl (with a measured pH of 1.55) was used for

dilution instead of Milli-Q water. The sample of 86 μM $[Fe^{II}(PAR)_2]$ in 40% aq

acetonitrile with 0.1 N HCl (pH 1.5) was found to be stable for at least 1 day. Calibration

standards at pH 1.5 were assayed by LC-MS in SIM mode at m/z 485. The results shown in Figure 3.10 reveal that the points do not yield a straight line. A variable wavelength detector was also coupled to the HPLC, and the plot of the peak height of the $[Fe^{II}(PAR)_2]$ absorbance at 400 nm vs iron concentration (Figure 3.11) was similar to that in Figure 3.10. Thus, the nonlinearity is not due to ion suppression in the ESI source. Examining the pK_a values of PAR (Table 2.4) indicates that at pH 1.5 two coordination sites of PAR are protonated, the pyridine nitrogen and the ortho hydroxyl. It was, therefore, decided to prepare $[Fe^{II}(PAR)_2]$ standards at higher pH.
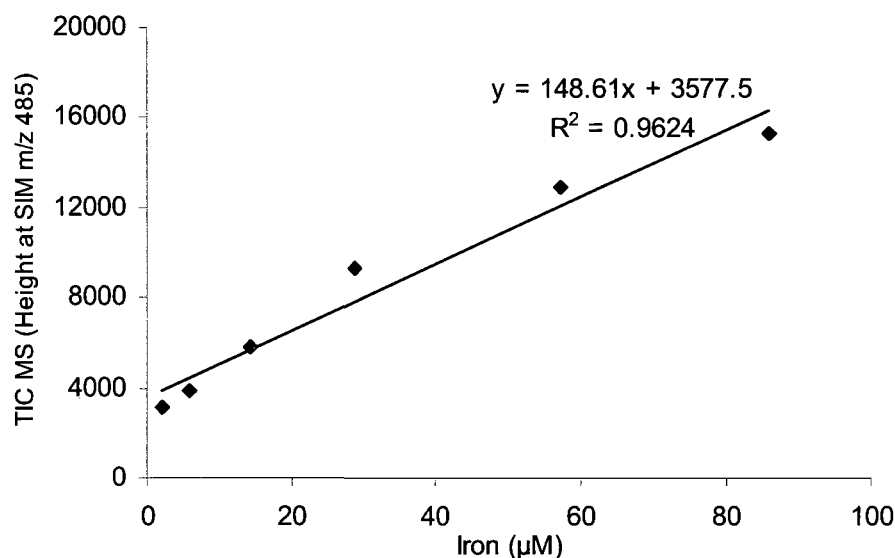
Figure 3.10: LC-MS standard curve of TIC at m/z 485 vs $[Fe^{II}(PAR)_2]$ concentration. A 10-µL aliquot of Fe^{III} standard with 223 µM PAR and 136 µM ascorbic acid in 40% aq acetonitrile/0.1 N HCl was injected onto an Agilent Technologies, Eclipse Plus C18 RRHT column (50 x 4.6 mm, 1.8 µm particle size at ambient column temperature). The mobile phase (40% aq 0.02% acetic acid/0.01% TFA in acetonitrile) was pumped at a flow rate of 1 mL/min and split at 120 µL/min to ion source through the HPLC system equipped with a variable-wavelength detector set at 400 nm. The heated capillary temperature was set at 350°C. The total run time was 2.4 min.
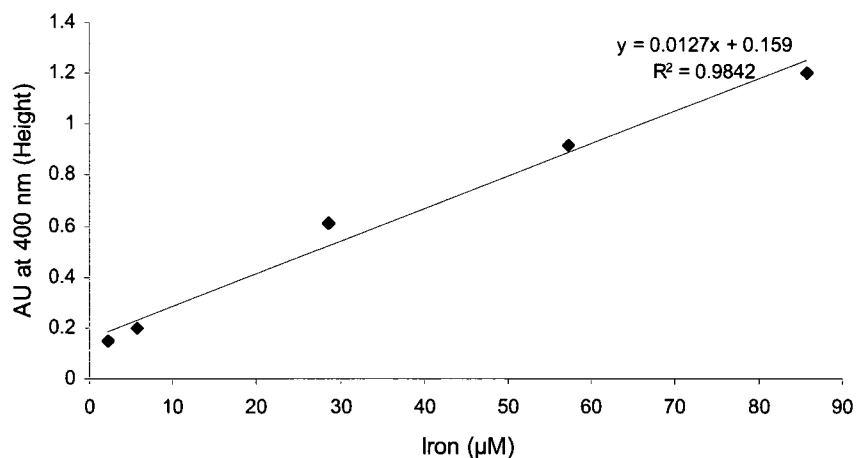
Figure 3.11: HPLC-UV (400 nm) calibration curve of standards from Figure 3.10.

$[Fe^{II}(PAR)_2]$ standards prepared in water (measured pH ~3) with 70% acetonitrile were found to be stable for at least 1 day. Consequently, $[Fe^{II}(PAR)_2]$ calibration samples prepared in 70% aq acetonitrile at pH 3 were injected into the LC-MS. The calibration curve in SIM mode at m/z 485 was not a straight line (Figure 3.12A) but a plot of peak height at 400 nm vs iron concentration exhibited good linearity with a high degree of correlation (Figure 3.12B). This suggests that there is an inherent problem with the MS method and not with the sample solutions. Thus, conditions suitable for MS analysis were researched.

Sample pH and mobile phase pH were varied to examine the effects on the standard curve. The sample pH was increased from pH ~ 3 to 5 by buffering with 20 mM ammonium acetate in order to deprotonate PAR and hence promote stronger complexation. The mobile phase pH was also increased to 4.5 from 3.3 to avoid pH mismatch. Unlike the evaluations in Sections 3.2 to 3.3, which utilized a single standard

solution (86 μM iron), three calibration points were plotted for each evaluation as shown in Figure 3.13. However, none of the curves produced straight lines.

Figure 3.12: LC-MS and HPLC-UV (400 nm) [Fe^{II}(PAR)$_2$] calibration curves in 70% aq acetonitrile. Peak heights vs iron concentration of (A) TIC in SIM mode at m/z 485 and (B) HPLC-UV absorbance at 400 nm. A 10-μL aliquot of Fe^{III} standard with 223 μM PAR and 136 μM ascorbic acid in 70% aq acetonitrile was injected onto an Agilent Technologies, Eclipse Plus C18 RRHT column (50 x 4.6 mm, 1.8 μm particle size at ambient column temperature). The mobile phase (40% aq 0.02% acetic acid/0.01% TFA in acetonitrile) was pumped at a flow rate of 1 mL/min and split at 120 μL/min to ion source through the HPLC system equipped with a variable-wavelength detector set at 400 nm. The heated capillary temperature was set at 350°C. The total run time was 2.4 min.
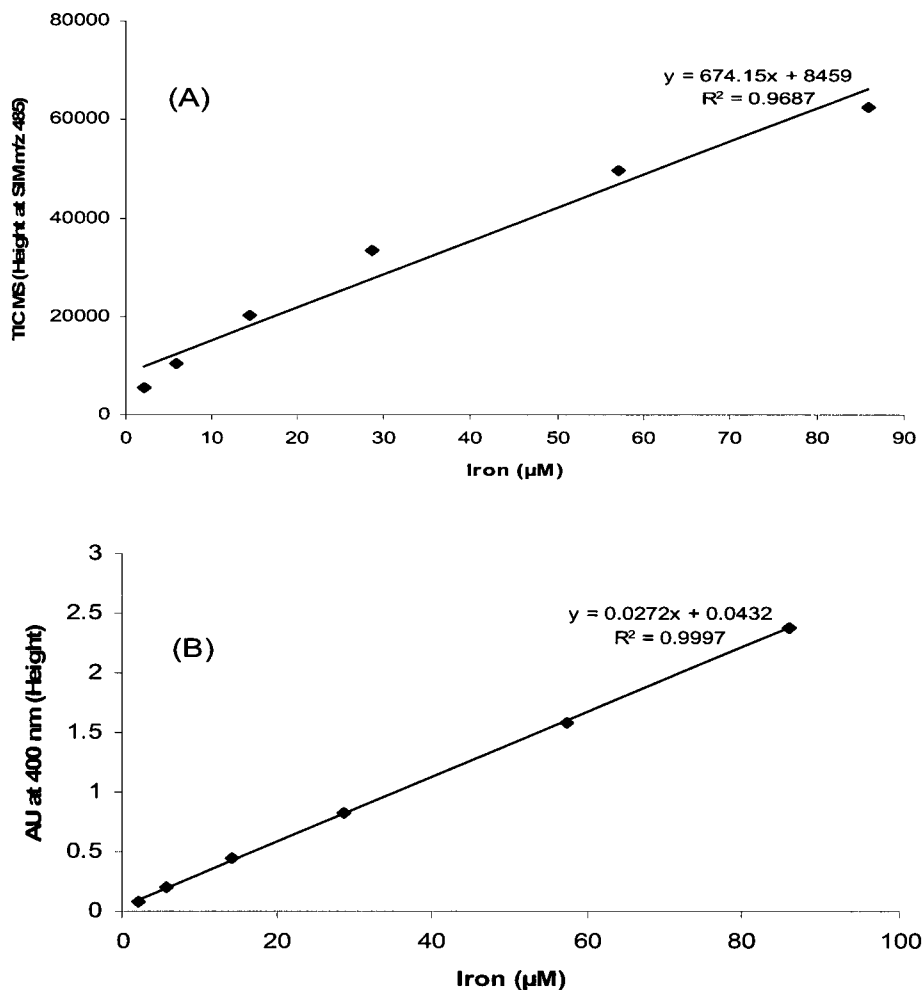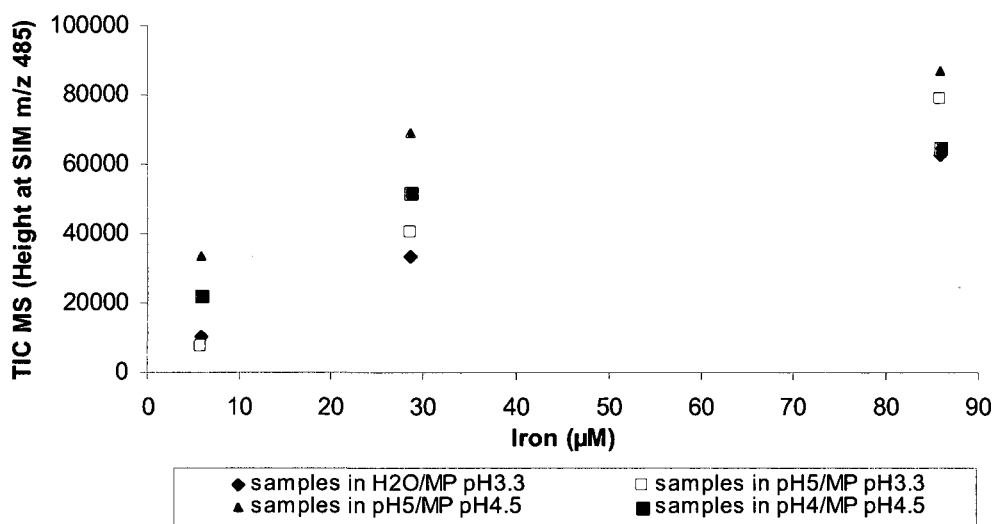
Figure 3.13: LC-MS [$Fe^{II}(PAR)_2$] calibration curves vs pH. Peak heights of TIC in SIM mode at m/z 485 were measured. A 10-μL aliquot of 6 μM, 29 μM, and 86 μM Fe^{III} standard with 223 μM PAR and 136 μM ascorbic acid in 40% aq acetonitrile was injected onto an Agilent Technologies, Eclipse Plus C18 RRHT column (50 x 4.6 mm, 1.8 μm particle size at ambient column temperature). The mobile phase (40% aq 0.02% acetic acid/0.01% TFA in acetonitrile) was pumped at a flow rate of 1 mL/min and split at 120 μL/min to ion source through the HPLC system equipped with a variable-wavelength detector set at 400 nm. The heated capillary temperature was set at 350°C. The total run time was 2.4 min.

Direct infusion of the samples solution into the mass spectrometer at a flow rate of 10 μL/min with a 250-μL Hamilton syringe was performed but this did not produce a straight line either (Figure 3.14), suggesting that PAR complexation with Fe^{II} may not be suitable for quantitative analysis by ESI-MS.
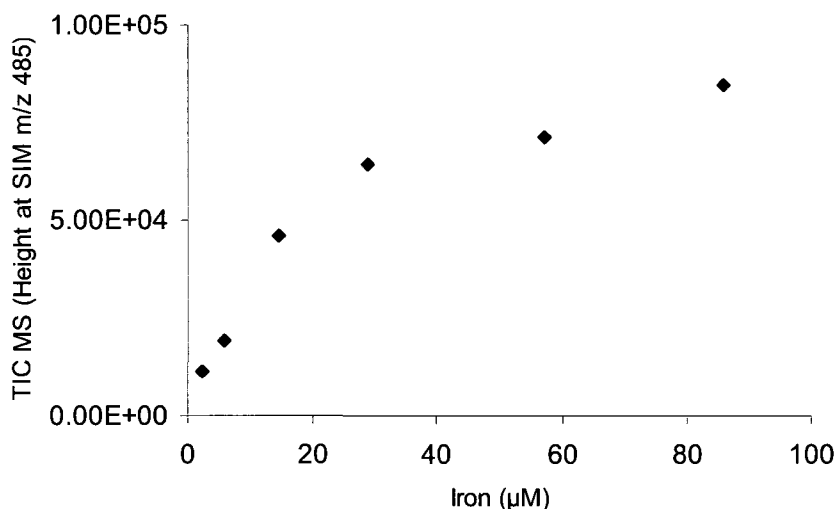
Figure 3.14: ESI-MS [Fe^{II}(PAR)$_2$] calibration curve. Following direct infusion of the standards into the mass spectrometer, peak heights in SIM mode at m/z 485 were measured. Solutions containing Fe^{III} standard and 223 μM PAR and 136 μM ascorbic acid in 40% aq acetonitrile were directly infused using a 250-μL Hamilton syringe at a flow rate of 10 μL/min. The scan time was 1 min and the heated capillary temperature was set at 350°C.

The [Fe^{II}(Phen)$_3$]$^{2+}$ complex was reinvestigated since Phen forms stable complex with Fe^{II} [39]. In Section 2.3.1, it was concluded that the [Fe^{II}(Phen)$_3$]$^{2+}$ complex is thermally labile at temperatures greater than 150°C. However, evaluation of the [Fe^{II}(Phen)$_3$]$^{2+}$ solutions in SIM mode at m/z 298 at 150°C also did not yield a good linear correlation (Figure 3.15). In addition, lowering the transfer capillary temperature to 150°C led to flooding of the ion source since desolvation was inefficient.
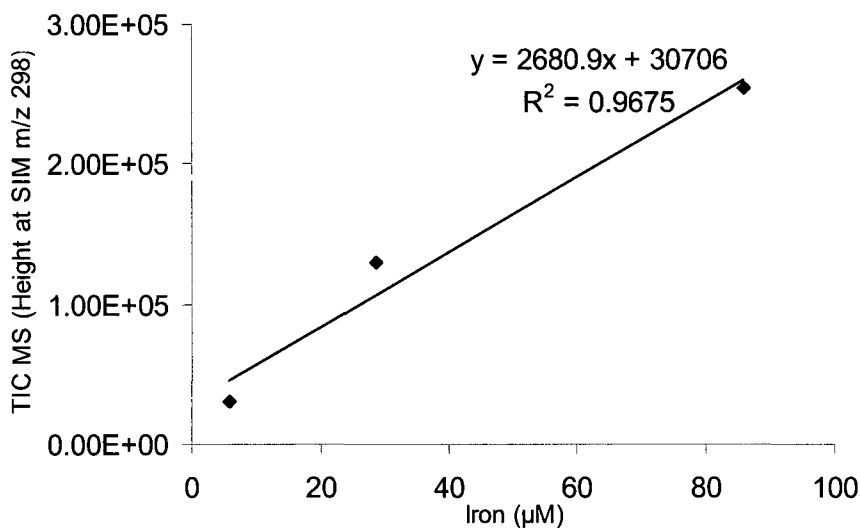
Figure 3.15: ESI-MS [Fe^{II}(Phen)$_3$]$^{2+}$ calibration curve. Following direct infusion of the standards into the mass spectrometer, peak heights in SIM mode at m/z 298 were measured. Solutions containing Fe^{III} standard and 404 µM Phen and 136 µM ascorbic acid in 40% aq methanol were directly infused using a 250-µL Hamilton syringe at a flow rate of 10 µL/min. The scan time was 1 min and the heated capillary temperature was set at 150°C.

Decreasing the calibration range to 43 µM [Fe^{II}(PAR)$_2$] did not yield a straight line (Figure 3.16A). However, the response from the variable wavelength detector at 400 nm revealed good linear correlation as shown in Figure 3.16B. This calibration equation was used to check the Qc samples, and the results (Table 3.3) were within the precision (1 – 3 %RSD) and accuracy (-1% to + 7%) criteria required by the US FDA guidelines (Table 2.6).

Efforts to establish a linear calibration curve for the [Fe^{II}(PAR)$_2$] complex did not succeed using MS detection. Presumably, the protonated [Fe^{II}(PAR)$_2$+H]$^+$ complex is not quantitatively formed in the ESI source. Despite the fact that ESI-MS is a sensitive and selective technique, many processes can occur during electrospray formation, such as

adduct formation, gas-phase ion reactions, and un-predictable ionization, all of which can lead to non-linear responses [16]. As a result of the nonlinear regression, MS quantitation of $[Fe^{II}(PAR)_2+H]^+$ in the SIM mode at m/z 485 is not feasible using an ESI source with a heated transfer capillary. However, quantitation by HPLC-UV/Vis would be possible based on the results in Figure 3.12B and Table 3.3.
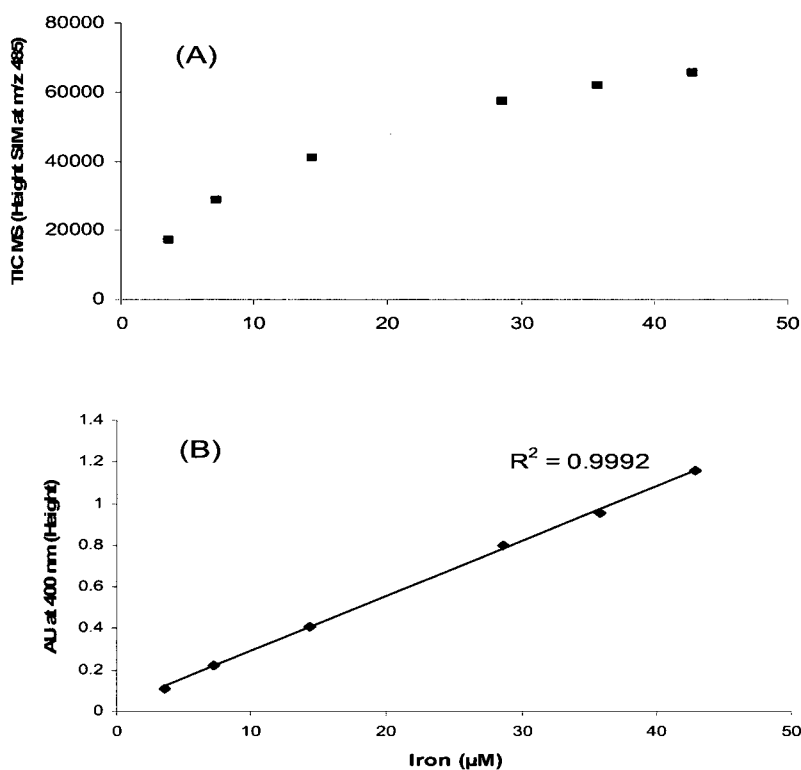
Figure 3.16: LC-MS and HPLC-UV (400 nm) [Fe^{II}(PAR)$_2$] calibration curves up to 43 μM iron. Peak heights vs iron concentration of (A) TIC in SIM mode at m/z 485 and (B) HPLC-UV absorbance at 400 nm. A 10-μL aliquot of Fe^{III} standard with 223 μM PAR and 136 μM ascorbic acid in 40% aq acetonitrile was injected onto an Agilent Technologies, Eclipse Plus C18 RRHT column (50 x 4.6 mm, 1.8 μm particle size at ambient column temperature). The mobile phase (40% aq 0.02% acetic acid/0.01% TFA in acetonitrile) was pumped at a flow rate of 1 mL/min and split at 120 μL/min to ion source through the HPLC system equipped with a variable-wavelength detector set at 400 nm. The heated capillary temperature was set at 350°C. The total run time was 2.4 min.

Table 3.3: Figures of merit for iron analysis as [Fe^{II}(PAR)$_2$] using HPLC-UV detection at 400 nm[a]

Qc sample μM[b]	Observed concentration μM[c]	% Difference[d]
5.71	5.79	1.46
	6.09	6.70
	6.09	6.58
Mean	5.99	4.90
%RSD[e]	2.89	
21.43	21.63	0.92
	22.15	3.38
	22.55	5.21
Mean	22.1	3.13
%RSD[e]	2.09	
39.29	38.94	-0.88
	39.29	0
	39.89	1.53
Mean	39.4	0.28
%RSD[e]	1.22	

[a] Experimental details are provided in the legend of Figure 3.16. [b] Target concentration of Qc sample. [c] Experimental results calculated using the calibration curve from Figure 3.16B. [d] (Experimental–Target)/Target x 100. [e] %RSD = Standard deviation/Mean x 100.

Chapter 4   General conclusions and suggestions for future work

This thesis has demonstrated metal ion analysis, such as the analysis of total iron described in Chapter 2, is one of many capabilities of ESI-MS. Despite an extensive literature on ESI-MS, only one publication was found that deals directly with quantitative metal-ion analysis using an ESI source [36]. ESI-MS has been shown here to be applicable to the analysis of total iron in pharmaceutical tablets containing iron oxide pigment. Since the method was developed for pharmaceutical applications, method validation figures of merit from an industry regulator, the US FDA, were followed and met (Section 2.4.3, Table 2.9).

Statistical analysis of the results obtained using ESI-MS and an instrument dedicated to metal-ion quantitation, ICP-OES, revealed no significant difference between the two methods, thus confirming the applicability of the ESI-MS in metal quantitation. The aim of the present study was not to replace elemental analysis performed with specialized and dedicated instruments such as ICP-MS/OES or AAS, but to provide an alternative to laboratories that require some metal-ion quantitation but do not have access to dedicated instruments for elemental analysis.

Karpinska and Kulikowska [7] increased the sensitivity of $[Fe^{II}(PAR)_2]$ detection to 0.14 µM using colorimetric analysis. This was accomplished by the transformation of the observed spectra into second-order derivatives, to decrease interference from other metal ions. Kolomiets et al. [6] established a linear range in colorimetric analysis from 1.43 µM to 10 µM $[Fe^{III}(PAR)_2]^+$ also using the second-order derivative of the absorbance. Yotsuyanagi et al. [23] achieved the same sensitivity as Karpinska and Kulikowska [7] by using EDTA to mask the interference, thus increasing the complexity

of the sample preparation. The dynamic range of the calibration curve established using colorimetric analysis by Vinogradov et al. [38] extended to 18 μM [$Fe^{II}(PAR)_2$]. The ESI-MS method developed here yields a LOD of 2 μM for [$Fe^{III}(PAR)_2$]$^+$, comparable to that achieved by Kolomiets et al. [6], without using masking reagents or raw-data transformation. ESI-MS is more specific than most colorimetric methods of iron analysis and in addition it is linear up to 43 μM for [$Fe^{III}(PAR)_2$]$^+$ (Figure 2.11). Furthermore, ESI-MS instrumentation is found in most pharma laboratories but a limitation of the instruments used here was the presence of the heated capillary.

As found in Chapter 3, a nonlinear response to [$Fe^{II}(PAR)_2+H$]$^+$ was observed using SIM mode at m/z 485. This may be due to the many variables associated with electrospraying a neutral complex molecule [16]. In addition, the use of excess ascorbic acid to reduce Fe^{III} to generate [$Fe^{II}(PAR)_2+H$]$^+$ could actually suppress the ionization, and yield the nonlinear response observed here. Despite this fact, the benefit of ESI-MS outweighs its limitation as shown in Chapter 2. Electrospraying of the pre-ionized [$Fe^{III}(PAR)_2$]$^+$ complex in 50% aq acetonitrile/0.1% formic acid, with the heated capillary temperature set at 350°C, yields a linear response over the range 2 – 43 μM total iron (Figure 2.11) in SIM mode at m/z 484. All method validation figures of merit were successfully met. Thus, the method can be applied in the analysis of total iron in pharmaceutical products containing iron oxide pigment.

Suggested future work is to investigate the mechanism by which PAR reduces Fe^{III}. The question also arises if PAR reduces or oxidizes other metal ions. The reduction of Fe^{III} observed in this thesis was implied by other researchers [23, 36], but no systematic examination of the properties of PAR complexes have been reported.

References

1. www.colorcon.com.

2. Piechocki J.T, Thoma K, *Pharmaceutical Photostability and Stabilization Technology*. 2006: CRC Press. 445.

3. Nyamweya N, Hoag S. W, Mehta K. A, *Film coating with aqueous latex dispersions: general considerations for formulating with pigments*, in *Pharmaceutical Technology*. 2001, 8-12, 26.

4. U.S. Department of Health & Human Services, USFDA, *Summary of Color Additives Listed for Use in the United States in Foods, Drugs, Cosmetics, and Medical Devices*. 2004.

5. Kemsley J, *Improving metal detection in drugs*, in *C&EN News*. 2008, 32-34.

6. Kolomiets L.L, Pilipenko L. A, Zhmud I. M, Panfilova I. P, *Application of derivative spectrophotometry to the selective determination of nickel, cobalt, copper, and iron(III) with 4-(2-pyridylazo) resorcinol in binary mixtures*. J. Anal. Chem. 1999, **54**(1), 28-30.

7. Karpinska J. Kulikowska M, *Simultaneous determination of zinc(II), manganese(II) and iron(II) in pharmaceutical preparations*. J. Pharm. Biomed. Anal. 2002, **29**(1), 153-158.

8. Ming X.Y, Wu Y. H, Schwedt G, *HPLC analysis of V, Co, Fe, and Ni by 4-(2-pyridylazo)resorcinol, PAR and H_2O_2 and studies on complex properties influencing retention*. Fresenius J. Anal. Chem. 1992, **342**(7), 556-559.

9.   Atanassova A., Lam R, Zamble D. B, *A high-performance liquid chromatography method for determining transition metal content in proteins.* Anal. Biochem. 2004, **335**(1), 103-111.

10.   Uluozlu O.D, Tuzen M, Mendil D, Soylak M, *Trace metal content in nine species of fish from the Black and Aegean Seas, Turkey.* Food Chem. 2007, **104**(2), 835-840.

11.   Omode P.E, Ademukola S. A, *Determination of Trace Metals in Southern Nigerian Honey by use of Atomic Absorption Spectroscopy.* Spect. Letters. 2008, **41**(7), 328-331.

12.   Kokot Z.J, Matysiak J, *Inductively coupled plasma mass spectrometry determination of metals in honeybee venom.* J. Pharm. Biomed. Anal. 2008, **48**(3), 955-959.

13.   Rattner B.A, Golden N. H, Toschik P. C, McGowan P. C, Custer T. W, *Concentrations of Metals in Blood and Feathers of Nestling Ospreys (Pandion haliaetus) in Chesapeake and Delaware Bays.* Arc. Environ. Contam. Tox. 2008, **54**(1), 114-122.

14.   Matsumoto K, Matsunami A, Oyama H, *Detection of Metal Oxides by MALDI/TOF MS.* J. Mass Spectrom. Soc. Jpn. 2004, **52**(6), 325-327.

15.   Siuzdak G, *The Expanding Role of Mass Spectrometry in Biotechnology.* 2003, MCC Press, 272.

16.   DiMarco V.B, Bombi G. G, *Electrospray Mass Spectrometry (ESI-MS) in the Study of Metal-Ligand Solution Equilibria.* Mass Spectrom. Rev. 2006, **25**(3), 347-379.

17.   Lobinski R, Schaumloffel D, Szpunar J, *Mass Spectrometry in Bioinorganic Analytical Chemistry.* Mass Spectrom. Rev. 2006, **25**(2), 255-289.

18.   Yamashita M. Fenn J. B, *Electrospray ion source. Another variation on the free-jet theme.* The J. of Phys. Chem. 1984, **88**(20), 4451-4459.

19.   Kenkel J, *Analytical Chemistry for Technicians.* 2003, CRC Press, 554.

20.   Koch S, Ackermann G, *The iron(III)/1,10-phenanthroline complex as a reagent for the determination of some anions and organic compounds.* Talanta. 1992, **39**(6), 687-691.

21.   Holzbecher Z, Divis L, Kral M, Sucha L, Vlacil F, *Handbook of Organic Reagents in Inorganic Analysis.* 1976, Ellis Horwood Ltd.

22.   Arya S.P, Mahajan M, Jain P, *Spectrophotometric determination of vitamin C using Fe(II)-1-(2-pyridylazo)-2-naphthol complex.* Indian J. Chem. 1999, **38**(A), 1303-1306.

23.   Yotsuyanagi T, Yamashita R, Aomura K, *Highly selective and sensitive spectrophotometric determination of iron(II) and cobalt(II) with 4-(2-pyridylazo)resorcinol (PAR).* Anal. Chem. 1972, **44**(6), 1091-1093.

24.   Harris D.C, *Quantitative Chemical Analysis.* 1982, W. H. Freeman and Co., 374.

25.   Ghasemi J, Seifi S, Sharifi M, Ghorbani R, Amini A, *Simultaneous kinetic spectrophotometric determination of ascorbic acid and L-cysteine by H-Point standard addition method.* Microchimica Acta. 2004, **148**(3-4), 259-265.

26.   Keki S, Nagy L, Torok J, Deak G, Zsuga M, *A simple method for estimating activation energies using the fragmentation yield: collision-induced dissociation*

of iron(II)-phenanthroline complexes in an electrosypray ionization mass spectrometer. J. Am. Soc. Mass Spectrom. 2006, **17**(7), 962-966.

27. http://www2.sisweb.com/mstools/isotope.htm.

28. http://www.fda.gov/cder/guidance/2396dft.htm, *Analytical Procedures and Methods Validation: Chemistry, Manufacturing and Controls Documentation.* 2000.

29. http://www.fda.gov/cder/guidance/4252fnl.htm, *Guidance for Industry: Bioanalytical Method Validation.* 2001.

30. Gardner C.B, Carey A. E, *Trace metal & major ion inputs into the Olentangy River from an urban storm sewer.* Environ. Sci. Tech. 2004, **38**(20), 5319-5326.

31. De B.K, Roberts W. L, *Performance characteristics of the Dimension RxL iron and total iron-binding capacity methods.* Clin. Chimica Acta. 2003, **333**(1), 51-57.

32. http://www.graphpad.com/quickcalcs/ttest1.cfm, *Student t-test calculator*, Prism.

33. Gupta N, Nigam P. C, *Kinetics and mechanism of the reaction between bis 4-(2-pyridylazo)resorcinol ferrate(III) complex and cyanide ion.* Trans. Metal Chem. 1988, **13**(5), 367-370.

34. Arya S. P, Mahajan M, Jain. P, *Spectrophotometric determination of Vitamin C with iron(II)-4-(2-pyridylazo)resorcinol complex.* Anal. Chimica Acta. 2001, **427**(2), 245-251.

35. Gavazov K, Simeonova Z, Alexandrov A, *Extraction spectrophotometric determination of vanadium in natural waters and aluminium alloys using pyridylazo resorcinol (PAR) and iodo-nitro-tetrazolium chloride (INT).* Talanta. 2000, **52**(3), 539-544.

36. Cucinotta V, Carusso R, Giuffrida A, Messina M, Maccarrone G, Torrisi A, *Separation and quantitation of metal ions by 4-(2-pyridylazo)resorcinol complexation in capillary electrophoresis-electrospray ionization mass spectrometry.* J. Chromatography A. 2008, **1179**(1), 17-23.

37. Jezorek J.R, Freiser H, *4-(Pyridylazo)resorcinol-based continuous detection system for trace levels of metal ions.* Anal. Chem. 1979, **51**(3), 373-376.

38. Vinogradov S.N, Kosinski T. F, Zak B, *Complexometric determination of iron in heme proteins with 4-(2-pyridylazo) resorcinol.* Anal. Biochem. 1982, **120**(1), 111-112.

39 Adhikamsetty R. K, Gollapalli N. R, Jonnalagadda S. B, *Complexation kinetics of Fe^{2+} with 1,10-Phenanthroline forming ferroin in acidic solutions.* Int. J. Chem. Kin. 2008, **40**(8), 515-523.